

# The $pd \leftrightarrow \pi^+t$ reaction around the $\Delta$ resonance

L. Canton<sup>1</sup> and W. Schadow<sup>2</sup>

<sup>1</sup>*Istituto Nazionale di Fisica Nucleare, Sezione di Padova, Via F. Marzolo 8, I-35131 Padova,*

*Italy*

<sup>2</sup>*Physikalisches Institut der Universität Bonn, Endenicher Allee 11-13, D-53115 Bonn, Germany*

## Abstract

The  $pd \leftrightarrow \pi^+t$  process has been calculated in the energy region around the  $\Delta$ -resonance with elementary production/absorption mechanisms involving one and two nucleons. The isobar degrees of freedom have been explicitly included in the two-nucleon mechanism via  $\pi^-$  and  $\rho$ -exchange diagrams. No free parameters have been employed in the analysis since all the parameters have been fixed in previous studies on the simpler  $pp \leftrightarrow \pi^+d$  process. The treatment of the few-nucleon dynamics entailed a Faddeev-based calculation of the reaction, with continuum calculations for the initial  $p-d$  state and accurate solutions of the three-nucleon bound-state equation. The integral cross-section was found to be quite sensitive to the NN interaction employed while the angular dependence showed less sensitivity. Approximately a 4% effect was found for the one-body mechanism, for the three-nucleon dynamics in the  $p-d$  channel, and for the inclusion of a large, possibly converged, number of three-body partial states, indicating that these different aspects are of comparable importance in the calculation of the spin-averaged observables.

PACS: 25.80-e, 25.80Ls, 25.10+s, 13.75-n

Typeset using REVTeX

## I. INTRODUCTION

Pion production/absorption on nuclear systems represents a complex, challenging problem, and this fact has been known since many years. In the attempt to explain the multitude of experimental results collected over more than 40 years by now, many different theoretical approaches have been proposed so far, with the aim to improve our understanding of these reactions and, more generally, of the hadronic phenomena.

The simplest approaches which have been employed assume a one-nucleon mechanism originated by the  $\pi$ NN vertex (generally – but not always – a Galilei invariant non relativistic reduction of the usual  $\gamma_5$  pion-nucleon interaction) and recast the transition amplitude in a DWIA formalism where the many-body aspects can be treated with different levels of approximations [1]. First-order corrections from the  $\pi$ -nucleus multiple scattering series leads to the two-nucleon mechanisms where a pion emitted from one nucleon scatters from another before leaving the whole nucleus.

The non-perturbative character of the hadronic interactions, together with the energy-momentum mismatch which forbids absorption on single, free nucleons and suppresses one-nucleon absorption on bound nucleons, makes these rescattering effects an important aspect which cannot be ignored for the reproduction of low-energy data. At the  $\Delta$ -resonance, however, most of the assumptions used in the early calculations were not applicable, and other phenomenological approaches have been developed.

A relevant success was encountered by the “deuteron” model, originally employed by Ruderman [2], where the  $pd \rightarrow \pi^+t$  cross section is directly linked to the  $pp \rightarrow \pi^+d$  experimental cross section, by means of suitable nuclear structure functions. This method has the considerable advantage to disentangle the question of the choice of the correct interaction mechanisms from the knowledge of the bound state wavefunctions. The theoretical uncertainties about the interaction mechanisms at the resonance are simply bypassed through the employment of the experimental  $pp \rightarrow \pi^+d$  cross section. The approach has been later refined by several authors, which soon addressed their attention to the main issues such

as the role of the distortion effects, sensitivity of the results with respect to the available model wave-functions, and generalization of the formalism from three-baryon systems to the many-nucleon  $A(p, \pi^+)A + 1$  case. A partial but representative sample of works developed along these lines is given in Refs. [3–5].

More recently, the analysis of the  $A(p, \pi^+)A + 1$  reaction in terms of the  $pp \rightarrow \pi^+d$  process has been extended to spin observables by Falk [6], by using the  $pp \rightarrow \pi^+d$  amplitude analysis of Bugg *et al.* [7], rather than the averaged cross-section data of earlier works. In most cases, an overall fair, qualitative agreement with the trend of the large bulk of experimental data has been found, indicating that the deuteron model even in its spin-dependent version may be considered a starting point for phenomenological studies which include spin-polarization data. This kind of approaches, however, suffers from a number of problems which limits possible future refinements and demands for more appropriate theoretical formulations. First, the model considers NN production mechanisms limited to the (dominant)  $1 \rightarrow 0$  isospin transition, while a complete model should take into account also the effects in the remaining isospin channels. Second, the amplitudes used for input are on-shell quantities, while in the theory the off-shell effects should be taken into account. Third, there is a certain arbitrariness in the kinematical constraints which define the energy parameter for the evaluation of the input 2N production amplitude; because of that, the results are not uniquely determined. And finally, in practically all applications the distortion contributions are in danger of double countings; indeed, in the evaluation of the distortion effects one should subtract the distortion contributions on the active pair, which are already included in the  $pp \rightarrow \pi^+d$  data.

To overcome these limitations, and to challenge the validity of the “deuteron” approaches, there has been a number of papers where more microscopic models have been suggested [8–10]. Here, the dynamical input was not mediated or hidden by the cross-section data, but consists of non-relativistic interactions among pions, nucleons, and isobars. In particular, the coupled  $\Delta N$  dynamics is obtained through the solution in R-space of the two-baryon Schrödinger equation. First calculations [8] employed simple s-wave deuteron and triton

wave-functions of uncorrelated gaussian forms, and were extremely limited in the number of intermediate states included in the calculation. Subsequent analyses [9,10] used better parameterizations (including  $d$  states) for the nuclear wave-functions, and increased slightly (from 1 to 4 or 5) the number of two-body angular-decomposed intermediate states, finding that these aspects improve the calculated angular distributions without, however, finding an agreement with theory and experiments, especially for the results at large angles, where considerable discrepancies persist. One of the conclusions from these studies was that these microscopic calculations needed important improvements in order to give a good reproduction in the normalization and in the angular distributions, and that these improvements would lead to enormous complications in the theoretical evaluation of the observables.

In an attempt to go beyond the description of meson production in terms of single-nucleon and two-nucleon mechanisms [11], it was shown that meson double rescattering could be a good candidate to account for the discrepancies at backward angles, particularly in the energy region above the  $\Delta$ -resonance. However, the bulk results, while moving towards the right direction, were still far from being optimal and this again poses the question of the need to overcome the various technical approximations which had to be assumed to keep the calculation tractable. The study has the merit to address the attention to the problem of three-body mechanisms in meson production/absorption, and this is still an open question which we hope will be theoretically disentangled in the near future with the help of the results collected in recent years by pionabsorption experiments with large angular detector systems [12–14] and by making comparative analyses in the  $\Delta$  region with the phenomenology of  $^3\text{He}$  photodisintegration [15].

In this paper, we have calculated the excitation function and differential cross-section for the  $pd \rightarrow \pi t$  reaction in the  $\Delta$  region by using single-nucleon and two-nucleon mechanisms. In particular, the two-nucleon mechanism explicitly refers to the intermediate isobar excitation with  $\pi + \rho$  exchange  $\Delta\text{N}$ - $\text{NN}$  transitions with tensor components. The one-body mechanism is mediated by the  $\pi\text{NN}$  vertex, while the two-body process is triggered by the  $\pi\Delta\text{N}$  one. The two mechanisms have been decomposed in complete three-nucleon partial

waves, while the asymptotic pion–nucleus plane wave has been kept three–dimensional. This choice leads to matrix elements with a large number of couplings between different three–body states and the technical complications involved has been kept under control with a great deal of numerical analysis. Also the intermediate three–baryon ( $\Delta$ NN) state has been represented in partial waves with inclusion of angular momenta up to  $l = 2$  for the  $\Delta$ N subsystem. However, in preliminary test calculations [16], the quality of the convergence has been checked up to  $l = 5$ . The antisymmetrization prescription for the three nucleons has been fully taken into account via the formalism of the permutation operators [17] and brings into the theory further mechanisms which differ from the leading ones by exchange diagrams. The matrix elements of the symmetrization permutator  $P$  involve a large number of couplings between different three–nucleon partial waves, and rather than invoking a drastical reduction of the number of states, we have accepted to deal with the numerical difficulties implied by the approach.

Following the formalism developed in Ref. [17] we have embedded these absorption operators in a Faddeev–based treatment of the three–nucleon dynamics. Accurate bound–state wavefunctions have been obtained with high–rank Faddeev–AGS calculations, and a suitable generalization of the quasiparticle method to absorption processes has been formulated in order to take into account the three–nucleon dynamics in the  $pd$  channel. This continuum calculation has been performed in the rank–one (separable) approximation and therefore is not as accurate as the bound–state wavefunction, but this is the first calculation which, to our knowledge, includes a Faddeev–based treatment of the initial–state three–body dynamics for the  $pd \rightarrow \pi + t$  process (and the other processes related by isospin symmetry).

Because of the above mentioned reasons, we think that the treatment illustrated in this work achieves several improvements with respect to the previous, pioneering, microscopic analyses. We have devoted section II to further discussions on these and other important aspects of our calculations, such as the treatment of the  $\Delta$  mass and width in the intermediate three–body ( $\Delta$ NN) Green’s function, and the inclusion of off–shell effects (for this second aspect, see also the discussion at the beginning of Sect. III). The remaining part of

Sect. III compares the results of our analysis with experiments and Sect. IV contains a brief summary and the conclusions.

## II. THEORY

We express the transition amplitude for the  $\pi^+t \leftrightarrow pd$  reaction by the following matrix element

$$A_d^{\text{tot}} = {}_{\mathcal{S}}\langle \Psi_d^{(-)} | \mathcal{A} | \Psi_{\text{BS}} \rangle_{\mathcal{S}} | \mathbf{P}_0^\pi \rangle, \quad (1)$$

where  $|\Psi_{\text{BS}}\rangle_{\mathcal{S}}$  represents the three-nucleon bound-state (BS) and  ${}_{\mathcal{S}}\langle \Psi_d^{(-)} |$  the three-body continuum state with ingoing boundary condition and with the deuteron  $d$  in the asymptotic channel. Both states are assumed to be properly antisymmetrized in the nucleonic coordinates and the state  $|\mathbf{P}_0^\pi\rangle$  is the pion-nucleus three-dimensional plane wave. In a previous exploratory calculation [16] the bound-state wavefunction calculated in Ref. [18] was used. That wavefunction originally was determined in Ref. [18] by solving the Faddeev equation with the Paris potential and with explicit allowance of the  $\Delta$  degrees of freedom and consisted of 48 three-baryon partial waves, of which 22 refer to purely nucleonic states. Because of the smallness of the remaining isobar states, only the nucleonic states were retained in the calculation of Ref. [16]. In the present calculation, we have independently recalculated the three-nucleon bound state for various realistic nuclear potentials, and the details of these calculations are illustrated in subsection II B.

The absorption mechanisms are specified by the operator  $\mathcal{A}$ . To avoid double countings, we avoided purely nucleonic intermediate states in  $\mathcal{A}$ . This is because we calculate the final-state interactions among the three nucleons using realistic NN potentials, without performing any kind of subtraction in the nuclear potential.

In this study we consider absorption mechanisms generated by pion-nucleon interactions in  $p$  waves as described by the  $\pi N\Delta$  and  $\pi NN$  vertices. The nonrelativistic interaction hamiltonians are

$$H_{\pi N\Delta} = \frac{f_{\pi N\Delta}}{m_\pi} \int d\mathbf{r} \rho(\mathbf{r})(\vec{S} \cdot \vec{\nabla})(\vec{\Phi}(\mathbf{r}) \cdot \vec{T}), \quad (2)$$

for the  $\pi N\Delta$  interaction, and

$$H_{\pi NN} = \frac{f_{\pi NN}}{m_\pi} \int d\mathbf{r} \rho(\mathbf{r})(\vec{\sigma} \cdot \vec{\nabla})(\vec{\Phi}(\mathbf{r}) \cdot \vec{\tau}), \quad (3)$$

for the  $\pi NN$  one. Here, the baryonic density is denoted by  $\rho(\mathbf{r})$ , while  $\vec{\Phi}(\mathbf{r})$  is the pionic isovector field. The quantities  $M$  and  $m_\pi$  are the nucleon and pion masses, respectively, while  $\vec{\sigma}$  and  $\vec{\tau}$  are the nucleon spin and isospin operators, and  $\vec{S}$  and  $\vec{T}$  are the corresponding generalization to the isobar–nucleon transition.

The  $\pi NN$  vertex defines the simplest one–body absorption mechanism and is sometimes referred to as the impulse approximation (IA) mechanism. However, this is suppressed because of energy–momentum mismatch, therefore two–nucleon mechanisms dominate. These are taken into account through the  $\Delta$ –rescattering process, where the  $\pi NN$ – $NN$  inelasticities are modeled through a  $\pi N\Delta$ – $\Delta N$ – $NN$  two-step transition. Here the first transition is triggered by the  $\pi N\Delta$  vertex given above, followed by an intermediate  $\Delta N$  propagation and by the  $\Delta N$ – $NN$  transition. The intermediate propagation of the isobar is described by the Green’s function

$$G_0 = \frac{1}{E + M - \mathcal{M}_\Delta - \frac{p^2}{2\mu_\Delta} - \frac{q^2}{2\nu_\Delta}}, \quad (4)$$

where  $E$  is given by the pion energy plus the target kinetic energy in the c.m. system. The Jacobi variables  $p$  and  $q$  are the pair  $\Delta N$  and spectator nucleon momenta, respectively. Correspondingly,  $\mu_\Delta$  and  $\nu_\Delta$  are the reduced masses of the pair and spectator–pair systems.  $\mathcal{M}_\Delta - M$  is the isobar–nucleon mass gap. Since the  $\Delta$ –isobar is not a stable particle but a resonance, its mass is endowed with an imaginary part  $\Gamma_\Delta$ , associated to the decay width of the isobar

$$\mathcal{M}_\Delta = M_\Delta - E_s - \frac{i}{2}\Gamma_\Delta(E), \quad (5)$$

with  $M_\Delta = 1232$  (MeV) and  $E_s$  being the energy–shift parameter. The energy dependence for  $\Gamma$  has been modeled phenomenologically in a previous analysis of the  $\pi d \leftrightarrow pp$  reaction

[19]. Here we use the same analytical expression which has been obtained in that analysis, with the  $\Gamma_\Delta$  energy dependence extracted by the condition

$$\sigma(E) = \frac{D}{(E - E_R)^2 + \frac{\Gamma_\Delta(E)^2}{4}}, \quad (6)$$

where  $\sigma(E)$  is the experimental excitation function for pion absorption on deuterons. In the numerical calculation, the fit to  $\sigma(E)$  obtained by Ritchie [20] has been used.

In a meson-exchange framework [21,22], the  $N\Delta$ - $NN$  transition potential can be obtained from the  $\pi$ - and  $\rho$ -exchange diagrams

$$\begin{aligned} V_{N\Delta} &= (V_{N\Delta}^\pi + V_{N\Delta}^\rho)(\vec{T}_1^\dagger \cdot \vec{\tau}_2) \\ V_{N\Delta}^\pi &= -\frac{g_\pi f_{\pi N\Delta}}{2Mm_\pi} (\vec{S}_1^\dagger \cdot \vec{Q})(\vec{\sigma}_2 \cdot \vec{Q})G(\omega_\pi) \\ V_{N\Delta}^\rho &= -\frac{(g_\rho + f_\rho)f_{\rho N\Delta}}{2Mm_\rho} (\vec{S}_1^\dagger \times \vec{Q}) \cdot (\vec{\sigma}_2 \times \vec{Q})G(\omega_\rho). \end{aligned} \quad (7)$$

The operator  $\vec{Q}$  is the baryon-baryon transferred momentum,  $m_\rho$  is the mass of the  $\rho$ -meson and the function  $G(\omega)$ , which describes the meson-exchange propagation, takes into account the mass difference between nucleons and isobars

$$\begin{aligned} G(\omega) &= \frac{1}{2\omega^2} + \frac{1}{2\omega(M_\Delta - M + \omega)} \\ &\simeq \frac{1}{2\omega^2} + \frac{1}{2\omega^2 + 2m_\pi(M_\Delta - M)}. \end{aligned} \quad (8)$$

Here,  $\omega$  is the relativistic energy of the exchanged meson and, as shown in the last expression, we have taken into account the  $\Delta N$  mass difference in an approximated way in order to obtain analytical expressions when performing the partial-wave expansion. Each meson-baryon coupling in the transition potential has been endowed with a phenomenological form factor of monopole type, with the exclusion of the  $\rho N\Delta$  coupling, where a dipole-type form factor was assumed.

Finally, we discuss how the three-nucleon dynamics can be incorporated into the theory, or equivalently, how we calculate  ${}_S\langle\Psi_d^{(-)}|$ . The method is similar to previous procedures developed to incorporate final-state interactions (FSI) in the photodisintegration of three-body systems [27,28,23–25]. First, we introduce the operator  $P_{23}$  which exchanges spin,



isospin and position coordinates of nucleons 2 and 3. We then introduce the cyclic and anti-cyclic permutation operators  $P_2$  and  $P_3$  respectively. They exchange the global coordinates of the three nucleons in the following manner  $123 \rightarrow 231$  and  $123 \rightarrow 312$ , and can be expressed in term of the pair exchange operators as  $P_2 \equiv P_{12}P_{23}$  and  $P_3 \equiv P_{13}P_{23}$ . This leads to the full permutator

$$P \equiv P_2 + P_3, \quad (9)$$

and the normalized symmetrizer  $S \equiv \frac{1+P}{\sqrt{3}}$ . It is now possible to derive the complete wavefunction in terms of the asymptotic channel wavefunction  ${}_1\langle\Phi_d|$  (the subscript “1” denotes antisymmetrization with respect to the pair made of nucleons labeled “2” and “3”)

$${}_S\langle\Psi_d^{(-)}| = {}_1\langle\Phi_d|(1 + \mathbf{T}G_0)S, \quad (10)$$

where the three-body operator  $\mathbf{T}$  satisfies a Faddeev-like equation

$$\mathbf{T} = Pt + PtG_0\mathbf{T} \quad (11)$$

( $t$  is the two-nucleon t-matrix).

We now define the Møller operator  $\Omega^{(-)\dagger} \equiv 1 + \mathbf{T}G_0$ , in which case

$${}_S\langle\Psi_d^{(-)}| = {}_1\langle\Phi_d|\Omega^{(-)\dagger}S. \quad (12)$$

This operator satisfies the Faddeev-like equation

$$\Omega^{(-)\dagger} = 1 + PtG_0\Omega^{(-)\dagger}, \quad (13)$$

and by its means the pion-disintegration amplitude can be rewritten as

$$A_d = {}_1\langle\Phi_d|\Omega^{(-)\dagger}S\mathcal{A}|\Psi_{\text{BS}}, \mathbf{P}_0^\pi\rangle. \quad (14)$$

Because of the two equations above, the full amplitude satisfies the integral equation

$$A_d = {}_1\langle\Phi_d|S\mathcal{A}|\Psi_{\text{BS}}, \mathbf{P}_0^\pi\rangle + {}_1\langle\Phi_d|PtG_0\Omega^{(-)\dagger}S\mathcal{A}|\Psi_{\text{BS}}, \mathbf{P}_0^\pi\rangle. \quad (15)$$

The first term on the right-hand side corresponds to the plane-wave contributions, while in the second term the NN rescatterings (to all orders) are singled out.

As is well known, when the two-body transition matrix is represented in a separable form, the Alt-Grassberger-Sandhas (AGS) equations [26] for neutron-deuteron scattering reduce to effective two-body Lippmann-Schwinger equations. The same happens for the calculation of final-state interaction effects in the photodisintegration of the triton ( $\gamma + t \rightarrow n + d$ ) [27,28,23–25], where one obtains a similar effective two-body Lippmann-Schwinger equation, the only difference being that the driving term of the  $n$ - $d$  scattering equation (*i.e.* the particle-exchange diagram, the so-called “Z”-diagram) is replaced by the off-shell extension of the plane-wave photoabsorption amplitude. Here, we use a similar scheme for pion absorption on the three-nucleon systems.

In order to accomplish this, we use the separable expansion method proposed by Ernst, Shakin, and Thaler (EST) [32] for representing a given NN interaction. The EST method is very reliable and has been tested in the past for bound-state [33,34] and scattering calculations [35–37]. In this approximation the original interaction is expressed in separable terms of the form

$$V = \sum_{\mu,\nu=1}^N |f_\mu\rangle \Lambda_{\mu\nu} \langle f_\nu|, \quad (16)$$

where  $N$  is the rank of the approximation. The detailed structure of the potential, the parameters for the formfactors  $|f_\mu\rangle$  and the interaction strength  $\lambda$  can be found in Ref. [36,37]. The input two-body transition matrix  $t$  is given as a series of separable terms

$$t = \sum_{\mu\nu} |f_\mu\rangle \Delta_{\mu\nu} \langle f_\nu|. \quad (17)$$

To simplify the notation, we restrict the sum above to just one value for the indices  $\mu$  and  $\nu$ , so that the transition matrix takes the rank-one form  $t = |f_1\rangle \Delta \langle f_1|$ . In  $\Delta$  as well as in the form factor  $|f_1\rangle$ , we have also omitted the proper energy dependence, but it must be remembered that when the two-body  $t$ -matrix is embedded in the three-particle space the correct energy dependence is upon  $E - (\frac{3g^2}{4M})$ , where the energy of the spectator nucleon

has to be subtracted. The separable representation reproduces the correct negative-energy bound-state pole of the two-body  $t$ -matrix (for the deuteron quantum numbers) if the form factor satisfies the homogeneous equation

$$VG_0(E_d)|f_1\rangle = |f_1\rangle, \quad (18)$$

and, within a normalization factor,  $G_0(E_d)|f_1\rangle$  is the deuteron wave  $|\Phi_d\rangle$ .

Use of the separable representation of the  $t$ -matrix input in the integral equation (15) leads to the effective two-body equation

$$A(q, E) = B(q, E) + \int q'^2 dq' V(q, q', E) \Delta(E - \frac{3q'^2}{4M}) A(q', E) \quad (19)$$

with the definitions

$$\begin{aligned} A(q, E) &= {}_1\langle f_1, q | G_0^{(+)} \Omega^{(-)\dagger} S \mathcal{A} | \Psi_{\text{BS}}, \mathbf{P}_0^\pi \rangle, \\ B(q, E) &= {}_1\langle f_1, q | G_0^{(+)} S \mathcal{A} | \Psi_{\text{BS}}, \mathbf{P}_0^\pi \rangle, \\ V(q, q', E) &= {}_1\langle f_1, q | G_0^{(+)} P | f_1, q' \rangle_1. \end{aligned} \quad (20)$$

Here,  $A$  and  $B$  represent the off-shell extension for the full and plane-wave pionabsorption amplitudes, respectively, while  $V$  is the effective two-body potential which represents the one-particle exchange diagram between different sub-cluster rearrangements.

These amplitudes are decomposed in three-nucleon partial waves, while the pion-nucleus incident wave is treated in three dimensions. Details on the employed representation were given elsewhere [17]. The representation of the three-body states is defined in momentum space and the partial-wave decomposition is discussed within the  $jI$  coupling scheme. The index  $\alpha$  refers to the whole set of quantum numbers (*i.e.* orbital momentum, spin, total angular momentum, and isospin of the pair  $(ls)j; t$ , of the spectator  $(\lambda\sigma)I; \tau$ , total angular momentum, isospin and associated third components  $JJ^z; TT^z$ ).

The absorption mechanisms we include in our calculation have the following structure:

$$B_E^\Delta(q', \alpha', E) = 2\sqrt{3}$$

$$\begin{aligned}
& \times \sum_{\alpha'', \alpha_\Delta, \alpha} \int p'^2 dp' p''^2 dp'' q''^2 dq'' p_\Delta^2 dp_\Delta p^2 dp q^2 dq \frac{f_1(\alpha', p') \langle p' q' \alpha' | P | p'' q'' \alpha'' \rangle}{E - \frac{3}{4} \frac{q'^2}{M} - \frac{p'^2}{M} + i\epsilon} \\
& \times \frac{\langle p'' q'' \alpha'' | V_{N\Delta} | p_\Delta q'' \alpha_\Delta \rangle}{E + (M - \mathcal{M}_\Delta) - \frac{q''^2}{2\nu_\Delta} - \frac{p_\Delta^2}{2\mu_\Delta}} \langle p_\Delta q'' \alpha_\Delta | H_{\pi N\Delta} | p q \alpha \rangle \langle p q \alpha | \Psi_{\text{BS}} \rangle, \tag{21}
\end{aligned}$$

and

$$\begin{aligned}
& B_D^\Delta(q', \alpha', E) = 2\sqrt{3} \\
& \times \sum_{\alpha_\Delta, \alpha} \int p'^2 dp' p_\Delta^2 dp_\Delta p^2 dp q^2 dq \frac{f_1(\alpha', p')}{E - \frac{3}{4} \frac{q'^2}{M} - \frac{p'^2}{M} + i\epsilon} \\
& \times \frac{\langle p' q' \alpha' | V_{N\Delta} | p_\Delta q' \alpha_\Delta \rangle}{E + (M - \mathcal{M}_\Delta) - \frac{q'^2}{2\nu_\Delta} - \frac{p_\Delta^2}{2\mu_\Delta}} \langle p_\Delta q' \alpha_\Delta | H_{\pi N\Delta} | p q \alpha \rangle \langle p q \alpha | \Psi_{\text{BS}} \rangle \tag{22}
\end{aligned}$$

for the  $\Delta$ -rescattering mechanisms, and

$$\begin{aligned}
& B_E^{I.A.}(q', \alpha', E) = \sqrt{3} \\
& \times \sum_{\alpha'', \alpha} \int p'^2 dp' p''^2 dp'' q''^2 dq'' p^2 dp q^2 dq \frac{f_1(\alpha', p') \langle p' q' \alpha' | P | p'' q'' \alpha'' \rangle}{E - \frac{3}{4} \frac{q'^2}{M} - \frac{p'^2}{M} + i\epsilon} \\
& \times \langle p'' q'' \alpha'' | H_{\pi NN} | p q \alpha \rangle \langle p q \alpha | \Psi_{\text{BS}} \rangle, \tag{23}
\end{aligned}$$

$$\begin{aligned}
& B_D^{I.A.}(q', \alpha', E) = \sqrt{3} \\
& \times \sum_{\alpha} \int p'^2 dp' p^2 dp q^2 dq \frac{f_1(\alpha', p') \langle p' q' \alpha' | H_{\pi NN} | p q \alpha \rangle \langle p q \alpha | \Psi_{\text{BS}} \rangle}{E - \frac{3}{4} \frac{q'^2}{M} - \frac{p'^2}{M} + i\epsilon}, \tag{24}
\end{aligned}$$

for the one-body IA mechanisms. Clearly, all these mechanisms add coherently to give the total amplitude. The subscripts “E” and “D” differentiate between exchange and direct mechanisms, respectively. The “D” mechanisms correspond to the probability that nucleon “1” is the free nucleon in the outgoing channel (hence nucleons “2” and “3” form a deuteron) while the other two cases (*i.e.* nucleon “2” or “3” as free outgoing particle) are assembled together in the “E” mechanisms. These exchanges in the rearrangement channel are performed by the permutation operator  $P$ . We refer to the appendix of Ref. [29] for details on the partial-wave matrix elements for this operator. Each  $\Delta$ -rescattering mechanism is multiplied by the factor  $2\sqrt{3}$  which arises from the multiplicity of the possible two-body mechanisms and by the normalization factor due to Pauli principle. The same considerations lead to the factor  $\sqrt{3}$  in the impulse approximation. We also observe that a coupled-channel

structure has to be intended for the deuteron form factor  $f_1(\alpha', p)$ , since the deuteron  $d$ -wave component is obviously taken into account in our calculation. However, these coupled orbital-momentum components of the pair must be summed up coherently.

We assume that such a sum (over the coupled  $l$ 's) is performed at the present stage, so that the index  $\alpha'$ , from now on, collectively denotes the set of quantum numbers  $s, j, t, \lambda, I, \tau, J, J^z, T$ , and  $T^z$ .

Finally, we observe that the direct contribution to the  $\Delta$ -rescattering term, Eq.(22), vanishes on-shell. (On-shell, the two-nucleon quantum numbers  $s, j$ , and  $t$  are fixed by the deuteron state, and the relative motion of the spectator  $q$  is fixed by total energy conservation.) This vanishing effect is due to isospin considerations, since the intermediate  $\Delta N$  pair cannot be directly coupled to a final deuteron-like ( $t = 0$ ) pair. It does couple, however, through the permutation operator  $P$  in the exchange contribution, as well as through final-state interactions, where one can well have isovector pairs in the intermediate states.

Once the total absorption amplitude  $A^{\text{tot}}(q, \alpha', E)$  has been obtained, the pion-absorption excitation function is given by

$$\sigma = \frac{c_{ps}}{2} \sum_{\alpha'} |A^{\text{tot}}(q, \alpha', E)|^2, \quad (25)$$

with phase-space factor

$$c_{ps} = (2\pi)^4 \frac{q}{P_\pi^0} \frac{E_\pi E_t E_N E_d}{E^{\text{tot}^2}}, \quad (26)$$

where

$$\begin{aligned} E_\pi &= \sqrt{m_\pi^2 + P_\pi^{0^2}} \\ E_t &= \sqrt{M_T^2 + P_\pi^{0^2}} \\ E_N &= \sqrt{M^2 + q^2} \\ E_d &= \sqrt{M_D^2 + q^2} \\ E^{\text{tot}} &= E_N + E_d = E_\pi + E_t. \end{aligned} \quad (27)$$

Here,  $M_D$ ,  $M_T$ , are the deuteron and three-nucleon masses, respectively. The momentum  $q$  is the on-shell momentum (in c.m. frame) of the outgoing nucleon.

Similarly, the unpolarized differential cross-section for the  $\pi^+t \rightarrow pd$  reaction is given by

$$\frac{d\sigma}{d\Omega}(\theta) = \frac{c_{ps}}{2} \sum_{K, K^z} \times \left| \sum_{J, J^z, \lambda} C(\lambda K J; \lambda^z K^z J^z) Y_{\lambda}^{\lambda^z}(\Omega) \sum_I (-)^{\lambda-I+K} \hat{K} \hat{I} \begin{Bmatrix} 1 & \frac{1}{2} & K \\ \lambda & J & I \end{Bmatrix} A^{\text{tot}}(\lambda, I, J, J^z; T, T^z) \right|^2 \quad (28)$$

where  $K$  is the channel-spin of the deuteron-nucleon system, *i.e.* the sum of the spins of the two fragments  $\mathbf{K} = \mathbf{j} + \sigma$ .

Finally, detailed balance gives the expression for the unpolarized cross section for the inverse (pion production) reaction,

$$\left[ \frac{d\sigma}{d\Omega}(\theta) \right]^{\text{production}} = \frac{1}{3} \left( \frac{P_{\pi}^0}{q} \right)^2 \left[ \frac{d\sigma}{d\Omega}(\theta) \right]^{\text{absorption}}, \quad (29)$$

where  $\theta$  is the c.m. angle of the deflected particle.

### A. Partial-wave absorption amplitudes

We outline here the basic ingredients we used for the calculation of the absorption amplitudes in partial waves. The section is mainly technical and can be ignored on a first reading, if one is not interested in the details of the calculation.

For brevity, out of the four mechanisms discussed previously, we have selected only two mechanisms, namely the exchange  $\Delta$ -rescattering, which is the dominant one, and the direct I.A. term. The remaining mechanisms, direct  $\Delta$ -rescattering and exchange I.A. have a similar structure and do not introduce any novelty.

To avoid unnecessary complications in the formulas, we give here the amplitudes on shell, *i.e.*, we have substituted  $|\Phi_d\rangle$  in place of  $G_0(E_d)|f_1\rangle$  and have denoted by  $u_{lsj}(p) \equiv u(p)$  the  $s$  and  $d$  component of the deuteron in momentum space. For the inclusion of the three-nucleon dynamics via the AGS equations, these same amplitudes have been extended off

shell (see Eq. (18)). To fix the notation, the exchange  $\Delta$ -rescattering amplitude in partial waves can be denoted as follows

$$B_E^\Delta = 2\sqrt{3} \langle u\alpha'q' | P\hat{\mathcal{A}}_1 | \Psi_{\text{BS}}, \bar{\alpha}, \mathbf{P}_0^\pi \rangle, \quad (30)$$

where  $q'$  is the c.m. momentum of the  $N$ - $d$  system,  $\mathbf{P}_0^\pi$  is the c.m. momentum of the  $\pi^+ t$  channel and denotes the beam axis or equivalently the  $z$ -axis. While the former is a one-dimensional variable in a fully decomposed partial-wave scheme, the latter is three-dimensional, since we decompose in partial waves only the baryonic coordinates, not the pionic one. The operator  $\hat{\mathcal{A}}_1$  represents the  $\pi N$ - $\Delta$  transition on nucleon labeled “2”, intermediate  $\Delta$  propagation, and a  $\Delta N$ - $NN$  transition between nucleons “2” and “3”, while nucleon “1” acts as spectator. The process is diagrammatically illustrated in Figure 1 of Ref. [17], while  $P$  is the three-body permutator previously introduced. For the detailed form of  $P$  in partial waves, we used the expression given in the appendix of Ref. [29].

With  $\alpha'$  we collectively denote the quantum numbers for the  $jI$  decomposition of the  $p$ - $d$  channel listed according to Eq. (3.2) of ref. [17], while with  $\bar{\alpha}$  the quantum numbers for the three-nucleon bound state in the  $LS$  scheme are assumed. The details of the calculation in this scheme can be found in Ref. [18], while similar calculations in the  $jI$  scheme are found *e.g.* in Refs. [30,31].

The resulting expression is

$$\begin{aligned} \langle u, \alpha', q' | P\hat{\mathcal{A}}_1 | \Psi_{\text{BS}}, \bar{\alpha}, \mathbf{P}_0^\pi \rangle &= \mathcal{F} \sum_{\substack{kl_1l'_1\alpha''\alpha_\Delta \\ L_\Delta S_\Delta S_z m}} \tilde{g}(\alpha'\alpha''kl_1l_2l'_1l'_2) \mathcal{T}(\alpha''\bar{\alpha}) \\ &\times \mathcal{B}(\alpha''\alpha_\Delta\bar{\alpha}L_\Delta S_\Delta S_z m) \mathcal{I}_1(\alpha'\alpha''\alpha_\Delta\bar{\alpha}kl_1l'_1L_\Delta S_\Delta S_z m), \end{aligned} \quad (31)$$

where

$$\mathcal{F} = \frac{iP_0^\pi(3M + m_\pi)f_{\pi N\Delta}^2 f_{\pi NN}}{72\pi^3 m_\pi^3 (M + m_\pi)\sqrt{\pi\omega_\pi}}, \quad (32)$$

$$\tilde{g}(\alpha'\alpha''kl_1l_2l'_1l'_2) = -\hat{l}\hat{s}\hat{j}\hat{t}\hat{\lambda}\hat{I}\hat{l}'\hat{s}'\hat{j}'\hat{t}'\hat{\lambda}'\hat{I}' \begin{Bmatrix} \frac{1}{2} & \frac{1}{2} & t \\ \frac{1}{2} & T & t' \end{Bmatrix}$$

$$\begin{aligned}
& \times \sum_{LS} (-)^L \hat{L}^2 \hat{S}^2 \left\{ \begin{array}{ccc} \frac{1}{2} & \frac{1}{2} & s \\ \frac{1}{2} & S & s' \end{array} \right\} \left\{ \begin{array}{ccc} l & s & j \\ \lambda & \frac{1}{2} & I \\ L & S & J \end{array} \right\} \left\{ \begin{array}{ccc} l' & s' & j' \\ \lambda' & \frac{1}{2} & I' \\ L & S & J \end{array} \right\} \\
& \times (-)^{k+\lambda'+l'_1} \left(\frac{1}{2}\right)^{l_1+l'_2} \left(\frac{3}{4}\right)^{l_2} \sqrt{\frac{(2l'+1)!}{(2l_1)!(2l_2)!}} \sqrt{\frac{(2\lambda'+1)!}{(2l'_1)!(2l'_2)!}} \\
& \times \sum_{ff'} \hat{f} \hat{f}' C(l_1 l'_1 f; 000) C(l f k; 000) C(l_2 l'_2 f'; 000) C(\lambda f' k; 000) \\
& \times \left\{ \begin{array}{ccc} l & f & k \\ f' & \lambda & L \end{array} \right\} \left\{ \begin{array}{ccc} l_1 & l_2 & l' \\ l'_1 & l'_2 & \lambda' \\ f & f' & L \end{array} \right\}, \tag{33}
\end{aligned}$$

$$\begin{aligned}
\mathcal{T}(\alpha' \bar{\alpha}) &= 96 \sqrt{30} (-)^{s'+j'+1+\bar{s}+\bar{t}} \hat{s}' \hat{l}' \hat{j}' \hat{t}' \hat{I}' \hat{S}' \hat{t}' \hat{T}' \\
& \times \left\{ \begin{array}{ccc} t' & \frac{1}{2} & \frac{1}{2} \\ 1 & \frac{3}{2} & \frac{1}{2} \end{array} \right\} \left\{ \begin{array}{ccc} \frac{1}{2} & \bar{t} & t' \\ \frac{1}{2} & T' & \bar{T} \end{array} \right\} \left\{ \begin{array}{ccc} 1 & \frac{1}{2} & \frac{3}{2} \\ \frac{1}{2} & t' & \bar{t} \end{array} \right\} C(1 \bar{T} T'; 1 - \frac{1}{2} \frac{1}{2}), \tag{34}
\end{aligned}$$

$$\begin{aligned}
\mathcal{B}(\alpha' \alpha_{\Delta} \bar{\alpha} L_{\Delta} S_{\Delta} S_z m) &= (-)^{s_{\Delta}+S_{\Delta}+\bar{T}} i^{l_{\Delta}-l'} \hat{s}_{\Delta}^2 \hat{l}_{\Delta} \hat{S}_{\Delta} \hat{L}_{\Delta} \left( \begin{array}{ccc} l' & 2 & l_{\Delta} \\ 0 & 0 & 0 \end{array} \right) \left\{ \begin{array}{ccc} 1 & \frac{1}{2} & \frac{3}{2} \\ \frac{1}{2} & s_{\Delta} & \bar{s} \end{array} \right\} \\
& \times \left\{ \begin{array}{ccc} 1 & \bar{s} & s_{\Delta} \\ \frac{1}{2} & S_{\Delta} & \bar{S} \end{array} \right\} \left\{ \begin{array}{ccc} j' & s' & l' \\ 2 & l_{\Delta} & s_{\Delta} \end{array} \right\} \left\{ \begin{array}{ccc} \frac{1}{2} & \frac{3}{2} & 1 \\ \frac{1}{2} & \frac{1}{2} & 1 \\ s' & s_{\Delta} & 2 \end{array} \right\} \left\{ \begin{array}{ccc} l_{\Delta} & s_{\Delta} & j' \\ \lambda' & \frac{1}{2} & I' \\ L_{\Delta} & S_{\Delta} & J' \end{array} \right\} \\
& \times C(L_{\Delta} S_{\Delta} J'; (J'_z - S_z) S_z J'_z) C(\bar{L} \bar{S} \bar{J}; (J'_z - S_z) S_z J'_z) C(1 \bar{S} S_{\Delta}; 0 S_z S_z) \\
& \times C(l_{\Delta} \lambda' L_{\Delta}; m(J'_z - S_z - m)(J'_z - S_z)) C(\bar{l} \bar{\lambda} \bar{L}; m(J'_z - S_z - m)(J'_z - S_z)), \tag{35}
\end{aligned}$$

and

$$\begin{aligned}
\mathcal{I}_1(\alpha' \alpha'' \alpha_{\Delta} \bar{\alpha} k l_1 l'_1 L_{\Delta} S_{\Delta} S_z m) &= q^{l_2+l'_2} \int_0^{\infty} p'^2 dp' p'^{l_1+l'_1} u_{l' s' j'}(p') \int_{-1}^1 dx \frac{P_k(x)}{p^{*l''} q^{*\lambda''}} \int_0^{\infty} p^2 dp \\
& \times \int_{-1}^1 d \cos \hat{\mathbf{P}} \frac{\mathcal{Q}_{l'' l_{\Delta}}^T(p^*, p_{\Delta})}{E - \frac{p_{\Delta}^2}{2\mu_{\Delta}} - \frac{q^{*2}}{2\nu_{\Delta}}} \Theta_{l_{\Delta} m}(\cos \hat{\mathbf{P}}_{\Delta}) \Theta_{\bar{l} m}(\cos \hat{\mathbf{P}}) \\
& \times \int_{-1}^1 d \cos \hat{\mathbf{Q}}' \Theta_{\lambda'' n}(\cos \hat{\mathbf{Q}}') \Theta_{\bar{\lambda} n}(\cos \hat{\mathbf{Q}}) \Psi_{\bar{\alpha}}(p, q). \tag{36}
\end{aligned}$$

In this last equation, all the relevant momenta are defined in terms of the channel momenta  $q'$  and  $P_0^{\pi}$  and of the integration variables through the formulas



$$\begin{aligned}
p^* &= \sqrt{\frac{1}{4}p'^2 + \frac{9}{16}q'^2 + \frac{3}{4}p'q'x}, \\
q^* &= \sqrt{p'^2 + \frac{1}{4}q'^2 - p'q'x}, \\
p_\Delta &= \sqrt{\left(\frac{3M+m_\pi}{6M+3m_\pi}P_0^\pi\right)^2 + p^2 + 2\frac{3M+m_\pi}{6M+3m_\pi}P_0^\pi p \cos \hat{\mathbf{P}}}, \\
\cos \hat{\mathbf{P}}_\Delta &= \frac{\frac{3M+m_\pi}{6M+3m_\pi}P_0^\pi + p \cos \hat{\mathbf{P}}}{p_\Delta}, \\
q &= \sqrt{\left(\frac{1}{3}P_0^\pi\right)^2 + q^{*2} + \frac{2}{3}P_0^\pi q^{*2} \cos \hat{\mathbf{Q}}'}, \\
\cos \hat{\mathbf{Q}} &= \frac{\frac{1}{3}P_0^\pi + q^* \cos \hat{\mathbf{Q}}'}{q}.
\end{aligned} \tag{37}$$

In Eq. (36)  $P_k(x)$  represents the Legendre polynomials,  $\Theta_{lm}(\cos \theta)$  denotes the associated Legendre functions (normalized according to Ref. [17]),  $\mathcal{Q}_{ll'}^T(p, p')$  represents linear combinations of II-kind Legendre polynomials (see Eq. (43) in Ref. [19]), originated by the  $\pi + \rho$  meson-exchange diagrams in the tensor  $\Delta N$ - $NN$  force, and finally  $\Psi_{\bar{\alpha}}(p, q)$  is the triton wavefunction in momentum space and in the  $LS$  scheme. In the same equation, it is also assumed that  $n = J'_z - S_z - m$ , while the identities  $l_1 + l_2 = l'$  and  $l'_1 + l'_2 = \lambda'$  hold in both Eqs. (33) and (36).

Similarly, the direct I.A. amplitude in partial waves can be expressed as follows

$$B_D^{I.A.} = \sqrt{3} \langle u\alpha'q' | H_{\pi NN} | \Psi_{BS}, \bar{\alpha}, \mathbf{P}_0^\pi \rangle, \tag{38}$$

with the  $\pi NN$  vertex acting on nucleon “2” as a one-body operator.

The calculation of this matrix element yields

$$\langle u, \alpha', q' | H_{\pi NN} | \Psi_{BS}, \bar{\alpha}, \mathbf{P}_0^\pi \rangle = \mathcal{F}_2 \sum_{L'S'S_z m} \mathcal{B}_2(\alpha' \bar{\alpha} L' S' S_z m) \mathcal{I}_2(\alpha' \bar{\alpha} L' S' S_z m), \tag{39}$$

where

$$\mathcal{F}_2 = \frac{iP_0^\pi(3M+m_\pi)f_{\pi NN}}{2\pi m_\pi(M+m_\pi)\sqrt{\pi\omega_\pi}}, \tag{40}$$

$$\begin{aligned}
\mathcal{B}_2(\alpha' \bar{\alpha} L' S' S_z m) &= (-)^{1+\bar{s}+s'+\bar{t}+t'+S'+T'} \hat{s} \hat{s}' \hat{t} \hat{t}' \hat{S} \hat{T} \hat{j}' \hat{I}' \hat{L}' \hat{S}' \\
&\times \begin{Bmatrix} \frac{1}{2} & \bar{t} & t' \\ \frac{1}{2} & T' & \bar{T} \end{Bmatrix} \begin{Bmatrix} 1 & \frac{1}{2} & \frac{1}{2} \\ \frac{1}{2} & t' & \bar{t} \end{Bmatrix} C(1\bar{T}T'; 1-\frac{1}{2}\frac{1}{2})
\end{aligned}$$

$$\begin{aligned}
& \times \begin{Bmatrix} \frac{1}{2} & \bar{s} & s' \\ \frac{1}{2} & S' & \bar{S} \end{Bmatrix} \begin{Bmatrix} 1 & \frac{1}{2} & \frac{1}{2} \\ \frac{1}{2} & s' & \bar{s} \end{Bmatrix} \begin{Bmatrix} l' & s' & j' \\ \lambda' & \frac{1}{2} & I' \\ L' & S' & J' \end{Bmatrix} \\
& \times C(L'S'J'; (J'_z - S_z)S_zJ'_z) C(\bar{L}\bar{S}\bar{J}; (J'_z - S_z)S_zJ'_z) C(1\bar{S}S'; 0S_zS_z) \\
& \times C(l'\lambda'L'; m(J'_z - S_z - m)(J'_z - S_z)) C(\bar{l}\bar{\lambda}\bar{L}; m(J'_z - S_z - m)(J'_z - S_z)) \quad (41)
\end{aligned}$$

and

$$\begin{aligned}
\mathcal{I}_2(\alpha'\bar{\alpha}L'S'S_zm) &= \int_0^\infty p'^2 dp' u_{l's'j'}(p') \int_{-1}^1 d \cos \hat{\mathbf{P}}' \Theta_{l'm}(\cos \hat{\mathbf{P}}') \Theta_{\bar{l}m}(\cos \hat{\mathbf{P}}) \\
&\times \int_{-1}^1 d \cos \hat{\mathbf{Q}}' \Theta_{\lambda'n}(\cos \hat{\mathbf{Q}}') \Theta_{\bar{\lambda}n}(\cos \hat{\mathbf{Q}}) \Psi_{\bar{\alpha}}(p, q). \quad (42)
\end{aligned}$$

As in the previous case, all the relevant momenta have to be expressed in terms of the channel momenta  $q'$  and  $P_0^\pi$  and of the integration variables

$$\begin{aligned}
p &= \sqrt{p'^2 + \left(\frac{3M + m_\pi}{6M + 3m_\pi} P_0^\pi\right)^2 - 2\frac{3M + m_\pi}{6M + 3m_\pi} P_0^\pi p' \cos \hat{\mathbf{P}}'}, \\
q &= \sqrt{q'^2 + \left(\frac{1}{3} P_0^\pi\right)^2 + \frac{2}{3} P_0^\pi q' \cos \hat{\mathbf{Q}}'}, \\
\cos \hat{\mathbf{P}} &= \frac{-\frac{3M + m_\pi}{6M + 3m_\pi} P_0^\pi + p' \cos \hat{\mathbf{P}}'}{p}, \\
\cos \hat{\mathbf{Q}} &= \frac{\frac{1}{3} P_0^\pi + q' \cos \hat{\mathbf{Q}}'}{q}. \quad (43)
\end{aligned}$$

## B. 3N Bound-state calculation

For the calculation of the three-body bound-state energy  $E_T$  and wavefunction  $|\Psi_{\text{BS}}\rangle$  we start from the Lippmann-Schwinger equation

$$|\Psi_{\text{BS}}\rangle = \lim_{\epsilon \rightarrow 0} i\epsilon G(E_T + i\epsilon)|\Psi_{\text{BS}}\rangle. \quad (44)$$

Using the resolvent equation

$$G(z) = G_\beta(z) + G_\beta(z) \bar{V}_\beta G(z) \quad (45)$$

and performing the  $\epsilon$ -limit we end up with

$$|\Psi_{\text{BS}}\rangle = G_{\beta}(E_T)(V - V_{\beta})|\Psi_{\text{BS}}\rangle, \quad (46)$$

where  $V$  is the total interaction summed over the pairs,  $V_{\beta}$  is the nuclear interaction of the pair labeled by  $\beta$ ,  $\bar{V}_{\beta}$  denotes  $V - V_{\beta}$ , and  $G_{\beta}$  is the channel resolvent for the two-cluster partition.

If we now introduce the position  $|F_{\beta}\rangle = (V - V_{\beta})|\Psi_{\text{BS}}\rangle$  and the relation  $V_{\gamma}G_{\gamma} = T_{\gamma}G_0$ , we obtain the celebrated equation

$$|F_{\beta}\rangle = \sum_{\gamma} (1 - \delta_{\beta\gamma}) T_{\gamma} G_0 |F_{\gamma}\rangle. \quad (47)$$

Here, the summation runs over all two-fragment partitions  $\gamma$ . The ‘‘form-factors’’  $|F_{\beta}\rangle$  are related to  $|\Psi_{\text{BS}}\rangle$  by

$$|\Psi_{\text{BS}}\rangle = \sum_{\gamma} G_0 T_{\gamma} G_0 |F_{\gamma}\rangle = \sum_{\gamma} |\Psi_{\gamma}\rangle, \quad (48)$$

where the  $|\Psi_{\gamma}\rangle$  are the standard Faddeev components. This can be shown by using the definition of  $|F_{\beta}\rangle$  and again the relation  $V_{\gamma}G_{\gamma} = T_{\gamma}G_0$ :

$$|\Psi_{\gamma}\rangle = G_0 T_{\gamma} G_0 |F_{\gamma}\rangle = G_0 V_{\gamma} G_{\gamma} |F_{\gamma}\rangle = G_0 V_{\gamma} G_{\gamma} (V - V_{\gamma})|\Psi_{\text{BS}}\rangle = G_0 V_{\gamma}|\Psi_{\text{BS}}\rangle. \quad (49)$$

The bound-state equation (47) has to be projected onto the three-body partial waves  $|pqlbJT\rangle$ . In this subsection we use the so called channel-spin coupling. The label  $b$  denotes the set of quantum numbers  $(\eta K \lambda)$ , where  $K$  and  $\lambda$  are the channel spin of the three nucleons [ with the coupling sequence  $(j, \sigma)K$  ] and the relative angular momentum between the two-body subsystem and the third particle, respectively. In this paper, the channel-spin coupling  $K$  has been already introduced in Eq. (28). Here, the total angular momentum of the three-nucleon system  $J$  is given by the coupling sequence  $(K, \lambda)$  while  $T$  has been already defined as the total isospin.  $l$  is the usual orbital angular momentum, and  $\eta = (s, j; t)$  collectively denotes the spin, angular momentum [ with the coupling sequence  $(l, s)j$  ], and isospin of the two-body subsystem. Defining

$$F_{\beta}^b(q) = \sum_l \int_0^{\infty} dp p^2 f_l(p) \langle pqlbJT | G_0 | F_{\beta} \rangle, \quad (50)$$

inserting the finite-rank form for the T-matrix, and using the Pauli principle, we obtain the one-dimensional equation

$$F^b(q) = \sum_{b'} \int_0^\infty dq' q'^2 \mathcal{AV}^{bb'}(q, q', E_T) \Delta^{b'}(E_T - \frac{3}{4}q'^2) F^{b'}(q'), \quad (51)$$

with

$$\mathcal{AV}^{bb'}(q, q', E_T) = 2 \sum_{l'l'} \int_0^\infty \int_0^\infty dp p^2 dp' p'^2 f_l(p) \langle pqlbJT | G_0 | p'q'l'b'JT \rangle f_{l'}(p'). \quad (52)$$

The recoupling coefficients for the coupling scheme herein employed can be directly found in Ref. [38], or alternatively, they can be obtained starting from other coupling schemes [29] by means of the usual transformation algebra.

Equation (51) can be treated as an eigenvalue problem. The energy is varied until the corresponding eigenvalue is 1. The ranks for the partial waves taken into account for the bound state calculations for the different potentials are listed in Table III. Results for the binding energies can be found in Table IV.

The whole wavefunction can now be calculated by either using Equation (48) or by applying the permutation operator  $P$  defined in Eq. (9) on one Faddeev component [29]

$$|\Psi_{\text{BS}}\rangle = (1 + P)|\Psi_1\rangle. \quad (53)$$

This second representation has the advantage to be explicitly independent from the T-matrix representation, and is therefore computationally more convenient when the rank of the representation becomes large. The high accuracy of the wavefunction has been shown in Refs. [33,34].

For the calculation of the Born terms as illustrated in the previous section, the wavefunction was transformed into the  $LS$  scheme via

$$\begin{aligned} & \langle ((l\lambda)L, (s\sigma)S)JJ^z | \\ &= \sum_{jK} (-1)^{l+s+\lambda+\sigma+L+S+2K} j \hat{L} \hat{S} \hat{K} \begin{Bmatrix} l & S & K \\ \sigma & j & s \end{Bmatrix} \begin{Bmatrix} l & S & K \\ J & \lambda & L \end{Bmatrix} \langle (((ls)j\sigma)K\lambda)JJ^z |. \end{aligned} \quad (54)$$

### C. 3N continuum calculation

In this section we briefly summarize the continuum calculation. As already mentioned the method used here is similar to the techniques developed to incorporate final-state interactions (FSI) in the photodisintegration of triton [27,28,23–25]. The only difference is the inhomogeneity, *i.e.*, the Bornterm, of Eq. (19). Thus, with this replacement our working program for photodisintegration has been easily modified for pionabsorption. Both programs are based on a program for  $n$ - $d$  scattering [38], which has been rewritten for the EST-method used here and the above replacement. The Faddeev results for the continuum presented here are all calculated using a rank-one representation of the two-body  $t$ -matrices in the kernel of the integral equation. In the case of photodisintegration it has been shown [39] that this is enough for the observables calculated.

In the case of the pionabsorption the Bornterm is much more complicated and has more structure than in the case of photodisintegration. To achieve the required accuracy we used 70 grid points in the  $q$  variable for each channel for the off-shell extension of the Bornterm. For details of the numerical solution of the integral equation we refer to Ref. [40].

## III. RESULTS

Our analysis of the  $pd \rightarrow \pi^+t$  reaction is essentially a *parameter free* analysis, because all the parameters of the model were fixed in previous studies [19,41] on the simpler  $\pi^+d \rightarrow pp$  reaction. This was possible because the character of the calculation is sufficiently microscopic that the tuning parameters are basic quantities such as coupling constants and cut-offs at the meson-baryon vertices. Obviously these very same parameters enter in both  $pp \leftrightarrow \pi^+d$  and  $pd \leftrightarrow \pi^+t$  reactions. We refer to the analyses of Refs. [19,41] for a more detailed discussion on the  $\pi^+d \rightarrow pp$  reaction; here we limit ourselves to summarize few aspects which are specific of this approach. The coupling constants for the  $\Delta$ -rescattering mechanism are the ones referring to the  $\pi NN$ ,  $\pi N\Delta$ ,  $\rho NN$  and  $\rho N\Delta$  vertices, which were taken from Table

B.1 of Ref. [42] (model III). The cut-off parameters (in MeV) of the four vertices are 1600, 900, 1200, and 1350, respectively, which are practically equivalent to the ones given in the same Table B.1 cited above.

In the analysis of pion absorption on deuterons which we used as input for our study, there were only two authentically phenomenological ingredients. First, the way the  $\Delta$ -resonance propagates in the intermediate states, and, second, the off-shell nature of the  $\pi NN$  and  $\pi N\Delta$  vertices when the pion is the asymptotic particle, and hence rigorously standing on its mass shell.

Concerning the first point, the resonance peak in the experimental pion-deuteron absorption cross-section is below the position of a free  $\Delta$  (as observed by  $\pi N$  scattering) by a few tenths of MeV. This effect could not be explained within the dynamical model, and therefore the  $\Delta$  resonance peak has been positioned downwards by introducing an energy shift parameter. Phenomenologically, the magnitude of this shift is of the order of 30-35 MeV; it has, however, to be increased of about 20 MeV, (see Refs. [19,41]) if the motion of the other nucleon is taken into account. As for the isobar width, this was fixed to 115 MeV at the resonance, and therefore corresponds to the value of the free resonance width. Note, however, that the resonance peak for pion absorption on deuteron is broader, being around  $\Gamma_0 = 150$  MeV [43,44]. This broadening of the width is fully described by the  $\pi d \rightarrow pp$  model calculation, once all the mechanisms, including FSI, are taken into account.

The second point with a certain deal of phenomenology concerns the off-shell nature of the pion-baryon vertices, in case the pion is the asymptotic particle. When the pion is on its mass shell, the extended structure of the  $\pi NN$  and  $\pi N\Delta$  vertices may be governed by the nucleon momentum, if the nucleon is the off-shell particle. The importance of including these baryonic off-shell effects has been pointed out also in a recent study of  $\pi N$  scattering [45]. Thus, the two vertices have been endowed with a form factor depending upon the momentum  $\mathbf{k}$  of the interacting nucleon,

$$F_{N,\Delta}(k) = \frac{\lambda_{N,\Delta}^2}{\lambda_{N,\Delta}^2 + k^2}. \quad (55)$$

For the two–nucleon system  $k^2$  corresponds to the square of the Jacobi coordinate  $\mathbf{p}$ , while for the three–nucleon system, an averaging over angles yields  $k^2 \simeq p^2 + 0.25q^2$ .

At the level of the two–nucleon system, the model has been tested against the enormous variety of experimental data collected for the  $\pi^+d \leftrightarrow pp$  reaction, and its strength and weakness, especially at the level of spin observables, have been thoroughly discussed in Refs. [19,41].

To exhibit the quality of the results at the level of the two–nucleon system, we report in Figure 1 the total production cross section for the  $pp \rightarrow \pi^+d$  reaction from threshold to above the  $\Delta$  resonance. The parameter  $\eta$  corresponds to the pion momentum (c.m.), in units of pion mass. The experimental data were extracted from a collection of Refs. [46–55]. All data have been converted into production data using the principle of detailed balance, if necessary, and in case of the data of Ref. [46], charge–independence considerations were applied. The full line is the result obtained with the Bonn  $B$  potential, and with the  $p$ –wave pion–nucleon mechanisms which, as discussed in the previous section, include both isobar and non–isobar degrees of freedom. Practically indistinguishable from the full line there is a dotted line corresponding to a similar calculation but with the Paris potential. The differences between the two curves slightly increase with energy and at the resonance peak the Paris result is less than 5% smaller than the Bonn  $B$  one.

The other two curves (dashed and dashed dotted, respectively) correspond to the additional inclusion of  $s$ –wave pion–nucleon interactions in the final state of the production process (or conversely in the initial state, for pion absorption). The leading contribution for this  $\pi N$ – $\pi N$  interaction was obtained via a  $\rho$ –meson exchange model in Ref. [41]. The two curves differ in the choice of the NN potential, the Bonn  $B$  being referred to by the dashed line, the Paris by the dotted–dashed curve.

The log scale emphasizes the threshold results, and shows that in order to achieve a correct reproduction of data over three orders of magnitude, the pion–nucleon interactions via  $\rho$ –meson exchange have to be considered as well. Note, however, that the process around the  $\Delta$  resonance is dominated by the  $p$ –wave mechanisms which are triggered by the  $\pi NN$

and  $\pi N\Delta$  vertices. On a linear scale, the threshold effects in pion production due to the  $s$ -wave mechanisms would appear smaller.

At this stage of our study of the  $pd \leftrightarrow \pi^+t$  process, we have excluded the  $\rho$ -mediated pion-nucleon interaction in  $s$ -wave, and limited the analysis around the  $\Delta$  resonance. Further work is needed to include the low-energy mechanisms, and to extend the calculation at the production threshold. In what follows we considered pion-nucleon interactions in  $p$ -waves only. However, both  $\Delta$  and non- $\Delta$  degrees of freedom were considered. We note, however, that we treat the pion-nucleus wave three-dimensionally and carefully calculate the relevant kinematical transformations from the pion-nucleus to the pion-nucleon variables. This requires additional integrations over angular variables in order to produce the absorption amplitudes (see Eqs. (36) and (42)). And, because of this, the total angular momentum  $J$  is not restricted, neither is the parity  $P$ , and thus we have taken into account a few  $J^P$  states:  $J = (\frac{1}{2})^\pm$ ,  $J = (\frac{3}{2})^\pm$ ,  $J = (\frac{5}{2})^\pm$ , and  $J = (\frac{7}{2})^\pm$ . For each of these three-body quantum numbers, one should consider in principle an infinite set of partial waves for the two-body subsystem, which matches a corresponding infinite set of partial waves for the spectator particle to give a fixed  $J^P$ . Clearly, a truncation over a limited number of states is necessary. Table 1 shows the smallest set of three-body partial waves which have been included in our calculation. Here, four two-nucleon states have been included, namely  $^1S_0$ ,  $^3S_1$ ,  $^3D_1$ , and  $^1D_2$ , while the maximum values considered for the orbital and angular momentum of the *spectator* were  $\lambda = 5$  and  $I = \frac{9}{2}$ , respectively, for a total amount of 82 states. Such three-body states are indicated in the table according to the notation  $^{2s+1}l_j \lambda_I$ .

All our calculations, unless otherwise explicitly indicated, have been performed with a much larger set. In particular, in calculating the matrix elements of the absorption/production matrix elements with exchange operator, we took into account 18 two-body partial waves  $^1S_0$ ,  $^3S_1$ ,  $^3D_1$ ,  $^1D_2$ ,  $^3P_0$ ,  $^1P_1$ ,  $^3P_1$ ,  $^3D_2$ ,  $^3P_2$ ,  $^3F_2$ ,  $^1F_3$ ,  $^3D_3$ ,  $^3G_3$ ,  $^3F_3$ ,  $^3G_4$ ,  $^1G_4$ ,  $^3F_4$ , and  $^3H_4$ . This, with the same cuts in the spectator quantum numbers  $\lambda$  and  $I$  specified as before, yields 34 channels for  $J^P = (\frac{1}{2}^\pm)$ , 58 for  $J^P = (\frac{3}{2}^\pm)$ , 70 for  $J^P = (\frac{5}{2}^\pm)$ , and 70 for



$J^P = (\frac{7}{2}^{\pm})$  for a grand total of 464 three-body states. In solving the Faddeev equations for the three-nucleon dynamics in the  $p$ - $d$  channel, of the 18 nucleon-nucleon waves we have included the first 10 states ( $j \leq 2$ ) since for these the NN state-dependent interaction was available.

Figure 2 shows the integral cross section (in  $\mu\text{b}$ ) of the  $pd \rightarrow \pi^+t$  reaction around the resonance. The  $x$ -axis dependence is upon the parameter  $\eta$ , which has been previously defined. The experimental bars were obtained with the help of a collection of data contained in Refs. [56,57]. To this collection, we have added the experimental results of Ref. [58] for  $\pi^-$  absorption on  ${}^3\text{He}$  at 64 and 119 MeV, assuming time reversal and charge symmetry. The full, dotted, and dashed lines differ among each other for the NN potential which has been used to generate the asymptotic bound states, *i.e.* the deuteron and triton. The three curves represent calculations with Bonn  $B$  (solid line), Bonn  $A$  (dotted), and Paris interactions. We find that at the peak the Paris results are smaller than the Bonn  $B$  results by almost 25%. This relative difference is substantially larger than the 5% difference obtained for the simpler  $pp \rightarrow \pi^+d$  reaction. Experimentally, the  $pd \rightarrow \pi^+t$  cross-section is smaller by a factor 80–85 with respect to the  $pp \rightarrow \pi^+d$  one. This large suppression, due to the small overlap of the deuteron wavefunction in the incoming channel with the pion production matrix elements, is fully reproduced by our calculations.

The unpolarized differential cross section is reported in Figure 3 for a variety of energies spanning the  $\Delta$  resonance. While Figure 2 shows the normalization of the cross section, in Figure 3 we have addressed our attention to the pure angular dependence and therefore all the curves are normalized to the experimental data. Thus, the three curves referring to 300 MeV (lab energy of the proton) have been multiplied by a factor. The full line, referring to the result with Bonn  $B$  potential, has been multiplied by 1.075, the dotted line (Bonn  $A$ ) by 1.016, and the dashed line (Paris) by 1.329. The three factors are due to the differences in normalization immediately perceived in Figure 2 for  $\eta = 1$ , which is the corresponding value for that energy.

At the resonance peak, the angular differences between the various NN potentials are practically zero. These differences, however, increase in moving away from the resonance in both directions. We find larger differences above the resonance, for backward angles. In particular, calculations with Paris potential seem to reproduce better the data at backward angles.

In the first sector ( $E = 300$  MeV) of the figure, the data were taken from the inverse absorption reaction,  $\pi^- \text{}^3\text{He} \rightarrow nd$  at 64 MeV, Ref. [58], using the detailed balance and charge symmetry. In the same picture we have reported also four points obtained from Ref. [63] for the production reaction at 305 MeV. The four points are clearly visible because they stand above the rest of the data set. From the same reference [63], we have taken also the data at 330 MeV, shown in the second sector, while the data at 382 MeV were obtained from pion absorption reactions at 119 MeV. In particular, data from both reactions  $\pi^- \text{}^3\text{He} \rightarrow nd$  (Ref. [58]) and  $\pi^+ t \rightarrow pd$  (Ref. [59]) have been included. The data at 450 and 500 MeV were taken from Ref. [60] using charge independence, and finally, at 605 MeV, we considered the older data of Ref. [61]. In terms of integrated cross-section, that last set of angular data corresponds in Figure 2 to the datum at  $\eta = 2.4$ , which has the largest error bar. Because of this, the large multiplicative factors we found at this energy (5.956 for Bonn *B*, 5.413 for Bonn *A*, and 7.982 for Paris) seem to be attributable more to normalization problems in the data, than to the model calculation. For all the remaining energies, the normalization factors were all well around one.

Table 2 compares for the three NN potentials the integrated cross-section calculated under various conditions. The first row exhibits the contribution arising from the sole  $\pi\text{NN}$  vertex (denoted IA, Impulse Approximation). In the second row (PWa), we show a plane-wave calculation which includes the isobar degrees of freedom via the  $\pi\text{N}\Delta$  vertex. In the third row, PWb, the number of intermediate NN states have been increased from 4 up to 18 two-body partial waves, and from the sole *S* state up to the *D* states in the  $\Delta\text{N}$  orbital momentum. The effect in the total cross section is about 3%; however, as shown in the next figure, there is a not large but sizeable change in the angular dependence. In a forthcoming

article we will show that certain spin observables like  $A_{y0}$  are extremely sensitive to the number of waves included in the intermediate states.

Finally, in the last two rows (IS Ia and IS Ib) the effect of 3–nucleon dynamics in the incoming channel has been taken into account with the Faddeev formalism. Similarly than in the previous two rows, these differ between each other for the number of intermediate states. In both cases, the effect of the three–nucleon dynamics yields an increase of about 4% or less. Around the same value for  $\eta$ , the  $pd \rightarrow \pi^+t$  cross–section extracted from Ref. [60] gives  $35 \pm 3.2 \mu b$  at  $\eta = 1.32$ , while data extraction from [58] gives  $32.7 \pm 8.0$  at  $\eta = 1.43$ .

Figure 4 shows the differential cross–section calculated for  $\eta = 1.36$  in various conditions, in comparison to the data obtained for  $\pi^o$  production at 350 MeV assuming charge independence [60]. The solid line is the solution of the Faddeev equation for the three–nucleon dynamics in the incoming channel. The corresponding plane–wave results are shown by the dotted line. The comparison shows that the three–nucleon dynamics have a relatively small effect on the differential cross–section. On a linear scale, the effect is more pronounced at forward angles, however, on a log scale it becomes evident that the overall effect is simply a rescaling of the curve, without changing the angular dependence. The dashed line shows the results obtained with a limited number of channels (a total of 82 instead of 464). Differences are seen at both forward and backward angles. It is therefore important to consider convergence with respect to the number of three–body states included in the calculation. Finally, the dashed–dotted line contains the effect of the sole nucleonic intermediate states. For reasons of visibility, these non–isobaric effects have been multiplied by a factor of 10. Overall the effect is small, but at backward angles its contribution is larger than 10%. The calculations shown in the figure were performed with the Paris interaction. Practically identical angular dependences have been obtained with the Bonn  $B$  and Bonn  $A$  potentials.

Finally, Figure 5 exhibits the dependence of the differential cross section upon the parameter  $\eta$  for forward and backward angles. Due to the smallness of the three–body effects, the calculations have been performed in plane–wave approximation. The theoretical results have been divided by 2 for comparison with the experimental data for  $\pi^o$  production ob-

tained at Saclay [62]. The Bonn  $B$  and Paris curves have been normalized at  $E = 350$  MeV to the data of Ref. [60].

#### IV. SUMMARY AND CONCLUSIONS

We have analyzed the  $pd \rightarrow \pi^+t$  reaction around the  $\Delta$ -resonance with a model calculation which explicitly includes isobar degrees of freedom and meson-exchange diagrams. The elementary production/absorption mechanisms were tested on the simpler  $pp \rightarrow \pi^+d$  reaction. In particular, the position and width of the isobar resonance were modeled to reproduce the excitation function of the  $pp \rightarrow \pi^+d$  process, and off-shell effects in the baryonic coordinates were taken into account in both  $\pi NN$  and  $\pi\Delta N$  vertices. The same absorption mechanisms (without further changes) have been embedded in a Faddeev-based treatment for the  $pd \rightarrow \pi^+t$  process, where the three-nucleon bound state and the three-nucleon continuum dynamics in the initial channel have been calculated using the Faddeev-AGS formalism. The computational method is similar to the one employed recently for the triton photodisintegration. We have checked our results against integral and differential cross-section data in the resonance region, finding that the unpolarized experimental data are reproduced reasonably well.

As for the excitation function, we have found that the resonance peak is reproduced within the errors without changing the isobar parameters in passing from  $pp$  pionproduction to the  $pd$  one. We have also found that the magnitude of the curve (*i.e.* the normalization of the cross section) is sensitive to the nucleon-nucleon interaction used as input for the 3N bound state wavefunction, with a 25% difference between the Bonn potentials and the Paris one. This sensitivity is larger by a factor of 5 with respect to the  $pp \rightarrow \pi^+d$  process. The results with the Paris potential were always smaller than those obtained with the Bonn potentials.

We have then analyzed the angular dependence of the differential cross-section in the energy region spread around the resonance peak. At the peak there are practically no

differences in the angular distribution with respect to the model selected for the nucleon–nucleon interaction. In moving away from the peak, the angular distributions begin to show some interaction dependence: the differences are larger at higher energies and backward angles. The calculation with the Paris potential seems slightly in better agreement with the general trend of the data at backward angles. Definitive conclusions, however, should be drawn only after the  $\pi$ N interactions in  $s$ -wave will be also included.

At the resonance peak we have singled out the role of non isobaric  $\pi$ N interaction in  $p$ -wave (the IA term), analyzed the convergence of the calculation with respect to the number of intermediate three-baryon partial waves included, and considered the effect of the three-body dynamics in the nucleon–deuteron channel. It turns out that the size of these effects are all comparable. Indeed, the contribution of the IA term with respect to the total cross section ranges from 2 to 4 % depending on the model interaction which has been used. Differences of the same size are found when the calculation performed with a strictly necessary set of partial waves is compared with converged results. Finally, by means of the Faddeev–AGS formalism, it was possible to ascribe a 4 % effect to the contribution due to the three-nucleon dynamics in the nucleon–deuteron channel. It is obvious that this is equivalent to say that for the inverse pionabsorption reaction, final state interactions contribute with the same 4% amount.

In conclusion, we have here confirmed the expectations, previously formulated in Refs. [17,64], that a careful embedding of the basic pion absorption/production matrix elements in a Faddeev–based treatment of the few-nucleon dynamics is a very important tool for understanding the hadronic processes in nuclei at intermediate energies. Once this point has been settled, it is possible to move further on with the same approach and tackle other, more refined experimental data underlining the pion few-nucleon systems.

Such aspects are, *e.g.*, the pionic absorption on the diproton [65], the wealth of experimental data involving polarization phenomena [6,60,63,66], the pion-induced reaction at energies around the pionic threshold [67], and, finally, the meson-absorption coincidence experiments ( $\pi^+$ ,pp) at non conjugated angles with the connected puzzle of the “genuine”

three-body mechanisms [68]. However, before that all these aspects can be theoretically disentangled, an important improvement is needed in our treatment (as well as in any other approach). This is connected with the role played by the pion–nucleon  $s$ –wave interaction (in both its isoscalar and isovector components) in multiple rescattering processes. Stated in other words, it is the role played by pion–nucleus final state interaction (or initial, depending on the selected direction in time). This aspect is still missing in the present treatment of the  $d(p,\pi^+)t$  process, but a flavour of its importance can be immediately perceived in the simpler case of the  $p(p,\pi^+)d$  reaction, by glancing at the dashed and dotted–dashed curves passing through the data in Figure 1.

#### ACKNOWLEDGMENTS

We thank G. Cattapan, P.J. Dortmans, G. Pisent, and J.P. Svenne for scientific discussions and interest at an early stage of this research project. L.C. wishes to acknowledge helpful discussions and correspondence with K. Amos, Q. Ingram, B. Mayer, J. Köhler, P. Weber, A. Lehmann, W. Falk, and D. Hutcheon. W. S. wishes to thank the warm hospitality of the University of Padova during several visits. The work of W. S. was supported by the INFN and the Deutsche Forschungsgemeinschaft under Grant No. Sa 327/23-1.

## REFERENCES

- [1] J. M. Eisenberg and D. S. Koltun, *Theory of Meson Interactions with Nuclei* (John Wiley & Sons, New York, 1980) 305.
- [2] M. Ruderman, Phys. Rev. **87**, 383 (1952).
- [3] C. H. Q. Ingram, N. W. Tanner, J.J. Domingo, and J. Rohlin, Nucl Phys. **B31**, 331 (1971).
- [4] H. W. Fearing, Phys. Rev. C **11**, 1210 (1975), Phys. Rev. C **11**, 1493 (1975), Phys. Rev. C **16**, 313 (1977).
- [5] M. P. Locher and H. J. Weber, Nucl Phys. **B76**, 400 (1974).
- [6] W. R. Falk, Phys. Rev. C **50**, 1574 (1994).
- [7] D.V. Bugg, A. Hasan, and R. L. Shypit, Nucl. Phys. **A477**, 546 (1988). D. V. Bugg, Nucl. Phys. **A437**, 534 (1985).
- [8] A. M. Green and E. Maqueda, Nucl. Phys. **A316**, 215 (1979).
- [9] A. M. Green and M. E. Sainio, Nucl. Phys. **A329**, 477 (1979).
- [10] M. E. Sainio, Nucl. Phys. **A389**, 477 (1979).
- [11] J. M. Laget and J. F. Lecomte, Phys. Lett. B **194**, 177 (1987).
- [12] G. Backenstoss *et al.*, Phys. Rev. Lett. **55**, 2782 (1985).
- [13] T. Altholz *et al.*, Phys. Rev. Lett. **73**, 1336 (1994).
- [14] G. Backenstoss *et al.*, Phys. Lett. B **379**, 60 (1996).
- [15] G. Audit *et al.*, Nucl. Phys. **A614**, 461 (1997).
- [16] L. Canton, G. Cattapan, P.J. Dortmans, G. Pisent, W. Schadow, and J.P. Svenne, Proc. of the *VI Workshop on Theoretical Nuclear Physics Problems* I. Bombaci, A Bonaccorso,

- A. Fabrocini, A. Kviessky, S. Rosati, and M. Viviani eds. Cortona, Italy, 45 (1995).
- [17] L. Canton, J. P. Svenne and G. Cattapan, *Phys. Rev.* **C48** 1562 (1993).
- [18] Ch. Hajduk, P. U. Sauer, and W. Strueve, *Nucl. Phys.* **A405**, 581 (1983).
- [19] L. Canton, G. Cattapan, P. J. Dortmans, G. Pisent, and J. P. Svenne, *Can. J. Phys.* **74**, 209 (1996).
- [20] B. G. Ritchie, *Phys. Rev. C* **28**, 926 (1983).
- [21] H. Sugawara and F. von Hippel, *Phys. Rev.* **172**, 1764 (1968).
- [22] M. Gari, G. Niephaus, and B. Sommer, *Phys. Rev. C* **23**, 504 (1981).
- [23] W. Sandhas, in *Few-Body Syst. Suppl.* **1**, 64 (1986).
- [24] W. Schadow, J. Richter, and W. Sandhas, in *14th Int. IUPAP Conf. on Few Body Problems in Physics*, ed. F. Gross (CEBAF, Virginia, 1994) p. 695
- [25] W. Schadow and W. Sandhas, *Phys. Rev. C* **55**, 1074 (1997).
- [26] E.O. Alt, P. Grassberger, and W. Sandhas, *Nucl. Phys.* **B2**, 167 (1967).
- [27] I.M. Barbour and A.C. Phillips, *Phys. Rev. C* **1**, 175 (1970).
- [28] B.F. Gibson and D. H. Lehman, *Phys. Rev. C* **11** 29 (1975).
- [29] D. Hüber, H. Kamada, H. Witała, and W. Glöckle *Few-Body Syst.* **16**, 165 (1994).
- [30] T. Sasakawa and S. Ishikawa, *Few-Body Syst.* **1**, 3 (1986).
- [31] W. Glöckle *The Quantum Mechanical Few-Body Problem* (Springer, Berlin, 1993).
- [32] D. J. Ernst, C. M. Shakin, and R. M. Thaler, *Phys. Rev. C* **8** 46 (1973), *Phys. Rev. C* **9**, 1780 (1974).
- [33] W. C. Parke, Y. Koike, D. R. Lehman, and L. C. Maximon, *Few-Body Systems* **11**, 89 (1991).



- [34] W. Schadow, W. Sandhas, and J. Haidenbauer, (to be published).
- [35] J. Haidenbauer and Y.Koike, Phys. Rev. C **34**, 1187 (1986).
- [36] Y.Koike, J. Haidenbauer, and W. Plessas, Phys. Rev. C **41**, 396 (1987).
- [37] T. Cornelius, W. Glöckle, J. Haidenbauer, Y. Koike, W. Plessas, and H. Witała, Phys. Rev. C **41**, 2538 (1990).
- [38] Th. Januschke, T. Frank, W. Sandhas, and H. Haberzettl, Phys. Rev. C **47**, 1401 (1993).
- [39] W. Schadow and W. Sandhas, (to be published).
- [40] Th. Januschke, Ph.D. thesis, BONN-IR-90-52, Universität Bonn, 1990.
- [41] P.J. Dortmans, L. Canton, and K.A. Amos J. Phys. G **23**, 479 (1997).
- [42] R. Machleidt, Adv. Nucl. Phys. **19**, 189 (1989).
- [43] T. Ericson and W. Weise, *Pions and Nuclei* (Clarendon Press, Oxford, 1988).
- [44] B. G. Ritchie, Phys. Rev. C **28**, 926 (1983).
- [45] C. Schütz, J.W. Durso, K. Holinde, and J. Specht, Phys. Rev. C **49**, 2671, (1994).
- [46] D.A. Hutcheon *et al.*, Nucl. Phys. **A535**, 618 (1991).
- [47] P. Heimberg *et al.*, Phys. Rev. Lett. **77**, 1012 (1996).
- [48] Carl M.Rose Jr., Phys. Rev. **77**, 1305 (1967).
- [49] B. G. Ritchie, T. D. Averett, D. Rothenberger, J. R. Tinsley, R. C. Minehart, K. Giovanetti, L. C. Smith, G. S. Blanpied, and B. M. Freedom, Phys. Rev. C **47**, 21 (1993).
- [50] B. G. Ritchie *et al.*, Phys. Rev. C **24**, 552 (1981).
- [51] B. G. Ritchie *et al.*, Phys. Rev. C **27**, 1685 (1983).

- [52] S.I Gogolev *et al.*, Phys. Lett. B **300**, 24 (1993).
- [53] D. Axen, G. Duesdieker, L. Felawka, Q. Ingram, and R. Johnson, Nucl. Phys. **A256**, 387 (1976).
- [54] C.Richard–Serre, W. Hirt, D. F. Meadsday, E. G. Michaelis, M. J. M. Saltmarch, and P. Skarek, Nucl. Phys. **B20**, 413 (1970).
- [55] J. Boswell, R. Altemus, R. Minehart, L. Orphanos, H. J. Ziock, and E. A. Wadlinger, Phys. Rev. C **25**, 2540 (1982).
- [56] H. Machner, Acta Physica Polonica B **24**, 1555 (1993).
- [57] H. Machner, Proc. of the *5<sup>th</sup> International Symposium on Meson–Nucleon Physics and the structure of the Nucleon* Eds. G. Höler, W. Kluge, B. M. K. Nefkens vol. I, p. 127 Boulder, Colorado, (1993).
- [58] P. Weber *et al.* Nucl. Phys. **A534**, 541, (1991); P. Weber, private communications.
- [59] P. Salvisberg *et al.*, Phys. Rev C **46**, 2172, (1992).
- [60] J.M. Cameron, P. Kitching, J. Pasos, J. Thekkumthala, R. Abegg, D. A. Hutcheon, C.A. Miller, S. A. Elbakr, and A. H. Hussein, Nucl. Phys. **A472**, 718 (1987).
- [61] E. Aslanides *et al.* Phys. Rev. Lett **39**, 1654 (1977).
- [62] C. Kerboul *et al.* Phys. Lett. B **181**, 28 (1986); B. Mayer, private communication.
- [63] G. J. Lolos, E. L. Mathie, G. Jones, E. G. Auld, G. Giles, B. McParland, P.L. Walden, W. Ziegler, and W. R. Falk, Nucl. Phys. **A386**, 477 (1982).
- [64] G. Cattapan and L. Canton, Phys. Rev. C **44**, 1784 (1991).
- [65] H. Toki and H. Sarafian, Phys. Lett. **119B**, 285 (1982); K. Otha, M. Thies, and T.-S. H. Lee, Ann. Phys. N.Y. **163**, 420 (1985); R. R. Silbar and E. Piassetzky, Phys. Rev. C **29**, 1116 (1984); O. V. Maxwell and C. Y. Cheung, Nucl. Phys. **A454**, 606 (1985);

- D. Zucić and N. Šimičević, *Few-Body Syst.* **8**, 95 (1990); J. A. Niskanen, *Phys. Rev. C* **43**, 36 (1991).
- [66] J. A. Niskanen, Proc. 5th Int. Symp. on Polarization Phenomena in Nuclear Physics, Santa Fe 1980, AIP Conf. Proc. **69**, 62 (1981); E. G. Auld, Proc. 5th Int. Symp. on Polarization Phenomena in Nuclear Physics, Santa Fe 1980, AIP Conf. Proc. **69**, 93 (1981).
- [67] A. Boudard *et al.*, *Phys. Lett.* **B214**, 6 (1988); M. A. Pickar, A. D. Bacher, H. O. Meyer, R. E. Pollock, and G. T. Emery, *Phys. Rev C* **46**, 397 (1992); V. N. Nikulin *et al.*, *Phys. Rev. C* **54**, 1732 (1996).
- [68] H. J. Weyer, *Phys. Rep.* **195**, 295 (1990); C.H.Q. Ingram, *Nucl. Phys.* **A553**, 573c (1993).

## FIGURES

FIG. 1. Excitation function for  $\pi^+$   $d$  production (in microbarn) from  $pp$  collisions. The parameter  $\eta$  corresponds to the pion momentum (c.m.) divided by the pion mass. The full line is the result obtained with Bonn  $B$  potential and with  $p$ -wave pion–nucleon interactions which includes both isobar and non–isobar degrees of freedom. Practically indistinguishable from the full line, there is a dotted line which correspond to a similar calculation but with Paris potential. The other two curves (dashed, and dashed–dotted, respectively) correspond to the inclusion of pion–nucleon initial state interaction in  $s$ -wave and differ between each other for the NN potential being used. The Bonn  $B$  in the dashed case, Paris in the dotted–dashed case.

FIG. 2. Excitation function of pion production via proton–deuterium collisions (in microbarn). The calculation includes also  $\Delta$  excitation and has been performed with the same parameters as in Figure 1.

FIG. 3. Differential cross–section for  $\pi^+$  production in proton–deuterium collision.

FIG. 4.  $\pi^+$ -production differential cross–section at  $\eta = 1.36$ . The full line shows the results with inclusion of nucleon–nucleon initial–state interactions. The dotted line represents the plane–wave calculation. The dashed line shows the results with a limited number of channels. The dashed–dotted line shows the contribution of the sole non–isobar degrees of freedom, magnified by a factor 10. All calculations were performed with the Paris potential.

FIG. 5. Unpolarized differential cross-section for  $\pi^0$  production in proton-deuterium collisions. Circles and triangles represent measurements taken at Saturne [62] at forward and backward (c.m.) angles, respectively. The solid and broken curves are forward-angle calculations with Bonn  $B$  and Paris potentials, respectively, the dashed and dotted-dashed curves are the corresponding backward-angle results.

TABLES

$J^P = \frac{1}{2}^-$	$J^P = \frac{1}{2}^+$	$J^P = \frac{3}{2}^-$	$J^P = \frac{3}{2}^+$	$J^P = \frac{5}{2}^-$	$J^P = \frac{5}{2}^+$	$J^P = \frac{7}{2}^-$	$J^P = \frac{7}{2}^+$
$^1S_0P_{\frac{1}{2}}$	$^1S_0S_{\frac{1}{2}}$	$^3S_1P_{\frac{1}{2}}$	$^3S_1S_{\frac{1}{2}}$	$^1D_2P_{\frac{1}{2}}$	$^1D_2S_{\frac{1}{2}}$	$^1D_2P_{\frac{3}{2}}$	$^1D_2D_{\frac{3}{2}}$
$^3S_1P_{\frac{1}{2}}$	$^3S_1S_{\frac{1}{2}}$	$^3D_1P_{\frac{1}{2}}$	$^3D_1S_{\frac{1}{2}}$	$^3S_1P_{\frac{3}{2}}$	$^3S_1D_{\frac{3}{2}}$	$^3S_1F_{\frac{5}{2}}$	$^3S_1D_{\frac{5}{2}}$
$^3D_1P_{\frac{1}{2}}$	$^3D_1S_{\frac{1}{2}}$	$^1D_2P_{\frac{1}{2}}$	$^1D_2S_{\frac{1}{2}}$	$^3D_1P_{\frac{3}{2}}$	$^3D_1D_{\frac{3}{2}}$	$^3D_1F_{\frac{5}{2}}$	$^3D_1D_{\frac{5}{2}}$
$^3S_1P_{\frac{3}{2}}$	$^3S_1D_{\frac{3}{2}}$	$^1S_0P_{\frac{3}{2}}$	$^1S_0D_{\frac{3}{2}}$	$^1D_2F_{\frac{3}{2}}$	$^1D_2D_{\frac{3}{2}}$	$^1D_2F_{\frac{5}{2}}$	$^1D_2D_{\frac{5}{2}}$
$^3D_1P_{\frac{3}{2}}$	$^3D_1D_{\frac{3}{2}}$	$^3S_1P_{\frac{3}{2}}$	$^3S_1D_{\frac{3}{2}}$	$^1S_0F_{\frac{5}{2}}$	$^1S_0D_{\frac{5}{2}}$	$^1S_0F_{\frac{7}{2}}$	$^1S_0G_{\frac{7}{2}}$
$^1D_2P_{\frac{3}{2}}$	$^1D_2D_{\frac{3}{2}}$	$^3D_1P_{\frac{3}{2}}$	$^3D_1D_{\frac{3}{2}}$	$^3S_1F_{\frac{5}{2}}$	$^3S_1D_{\frac{5}{2}}$	$^3S_1F_{\frac{7}{2}}$	$^3S_1G_{\frac{7}{2}}$
$^1D_2F_{\frac{5}{2}}$	$^1D_2D_{\frac{5}{2}}$	$^1D_2P_{\frac{3}{2}}$	$^1D_2D_{\frac{3}{2}}$	$^3D_1F_{\frac{5}{2}}$	$^3D_1D_{\frac{5}{2}}$	$^3D_1F_{\frac{7}{2}}$	$^3D_1G_{\frac{7}{2}}$
		$^3S_1F_{\frac{5}{2}}$	$^3S_1D_{\frac{5}{2}}$	$^1D_2F_{\frac{5}{2}}$	$^1D_2D_{\frac{5}{2}}$	$^1D_2F_{\frac{7}{2}}$	$^1D_2G_{\frac{7}{2}}$
		$^3D_1F_{\frac{5}{2}}$	$^3D_1D_{\frac{5}{2}}$	$^3S_1F_{\frac{7}{2}}$	$^3S_1G_{\frac{7}{2}}$	$^3S_1H_{\frac{9}{2}}$	$^3S_1G_{\frac{9}{2}}$
		$^1D_2F_{\frac{5}{2}}$	$^1D_2D_{\frac{5}{2}}$	$^3D_1F_{\frac{7}{2}}$	$^3D_1G_{\frac{7}{2}}$	$^3D_1H_{\frac{9}{2}}$	$^3D_1G_{\frac{9}{2}}$
		$^1D_2F_{\frac{7}{2}}$	$^1D_2G_{\frac{7}{2}}$	$^1D_2F_{\frac{7}{2}}$	$^1D_2G_{\frac{7}{2}}$	$^1D_2H_{\frac{9}{2}}$	$^1D_2G_{\frac{9}{2}}$
				$^1D_2G_{\frac{9}{2}}$	$^1D_2H_{\frac{9}{2}}$		

TABLE I. Example of three–nucleon partial waves included in our calculation. The notation is  $^{2s+1}l_j \lambda_I$ , where  $s, l, j$  are spin, orbital, and total momentum of the pair, while  $\lambda$  and  $I$  are orbital and total momentum for the spectator nucleon. This set of 82 states corresponds to the inclusion of 4 two–nucleon states. In our actual calculation 464 three–body partial waves have been considered, corresponding to the inclusion of 18 two–nucleon states.

	Bonn <i>A</i>	Bonn <i>B</i>	Paris
IA	0.58	0.72	0.93
PWa	30.1	28.0	21.7
PWb	30.7	28.7	22.5
IS Ia	31.3	29.0	22.5
IS Ib	32.0	29.9	23.4

TABLE II. Calculated production cross sections (in microbarns) at  $\eta = 1.36$  for various NN potentials. The Impulse Approximation (first row) represents a bare plane-wave calculation without  $\Delta$  rescatterings. The second and third rows include also the  $\Delta$  degrees of freedom but use a plane-wave approximation in the incoming channel. They differ between each other for the number of partial waves included in the intermediate states. In case *a*, 4 two-nucleon states have been included and only *S*-wave orbital momentum for the intermediate  $\Delta$ -nucleon state has been considered. In case *b*, 18 two-nucleon states and intermediate  $\Delta$ -nucleon states in *S*, *P*, and *D* waves have been taken into account. In the last two rows, where the same number of partial waves have been included as in the previous two, the *p-d* interactions in the initial state have been included via a Faddeev calculation.

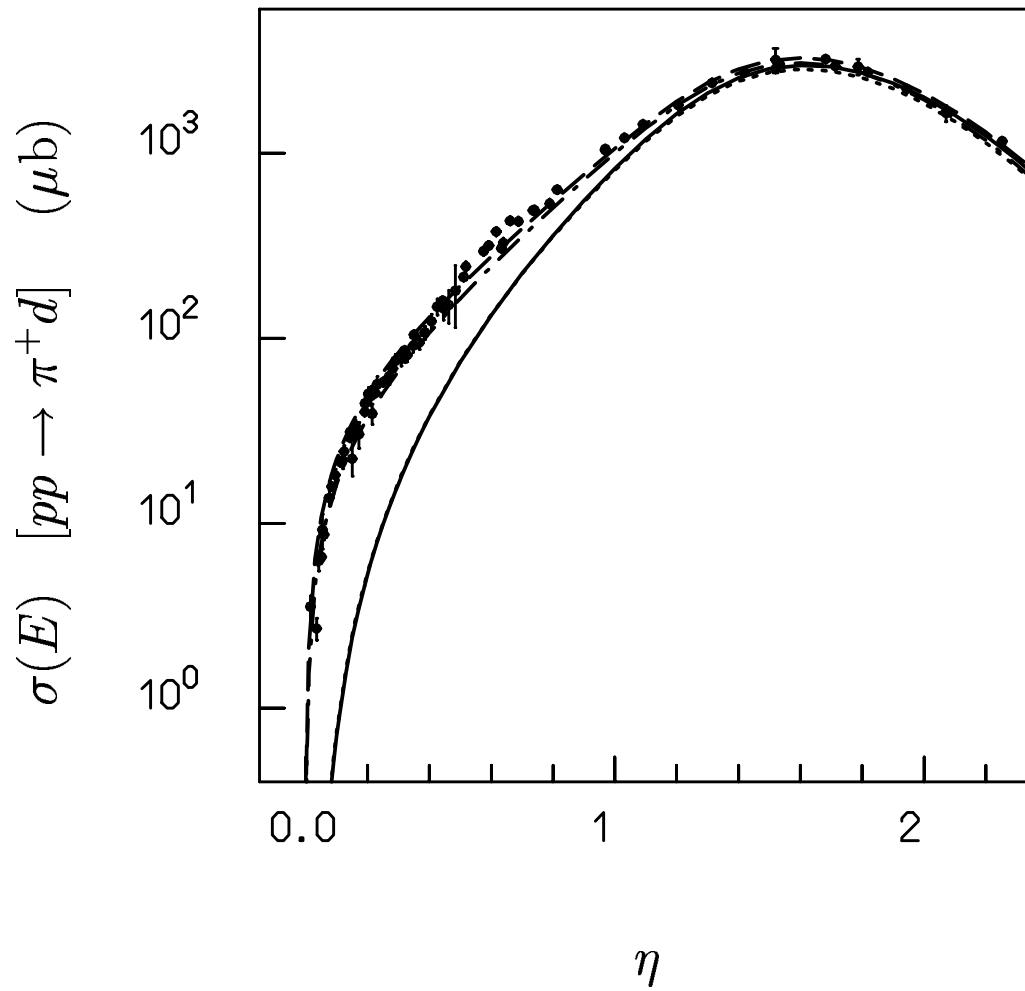
partial-wave	PEST	BAEST	BBEST
$^1S_0$	5	5	5
$^3S_1 - ^3D_1$	6	6	6
$^1D_2$	5	4	4
$^3D_2$	5	4	4
$^1P_1$	5	4	4
$^3P_1$	5	4	4
$^3P_0$	5	4	4
$^3P_2 - ^3F_2$	7	5	5

TABLE III. Ranks of the two-body partial-waves of the Paris, Bonn  $A$ , and Bonn  $B$  potentials in the EST-representation.

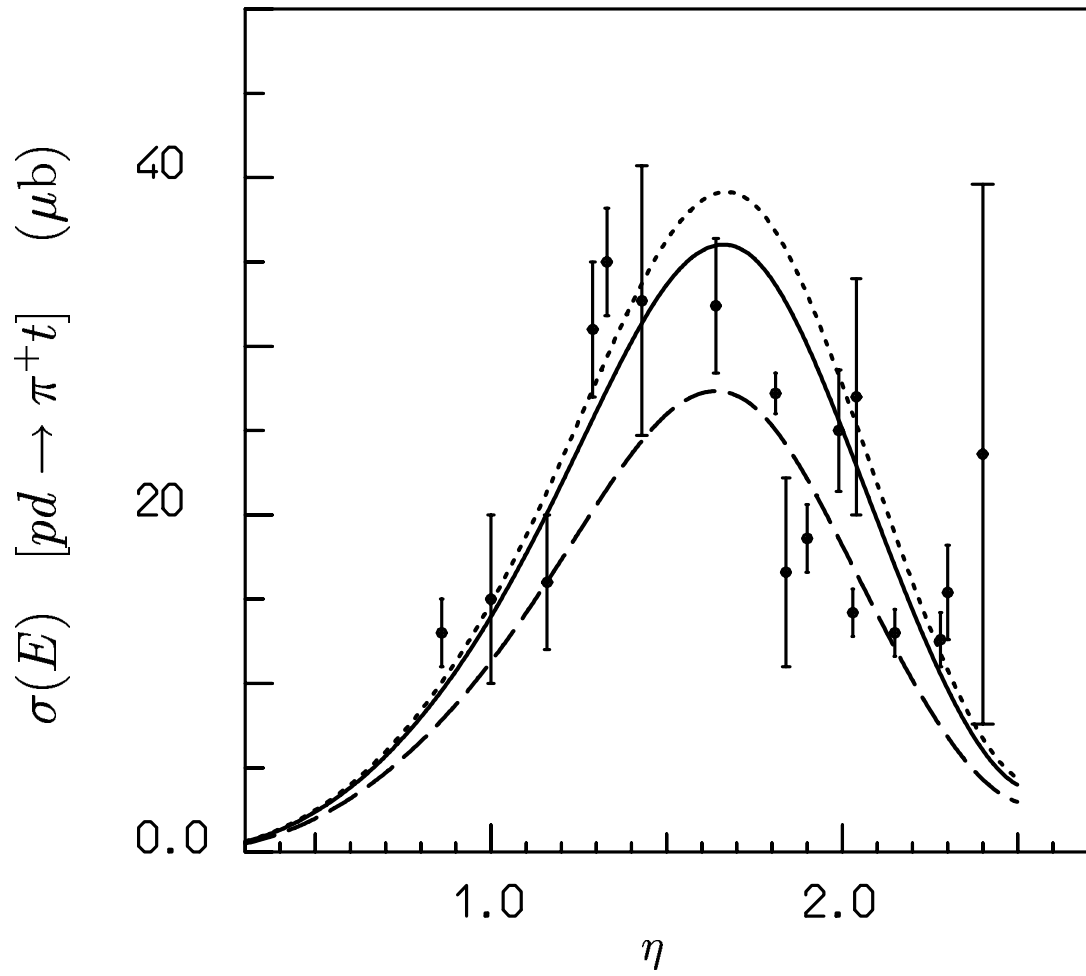
BAEST	BBEST	PEST
-8.284	-8.088	-7.3688

TABLE IV. Calculated binding energies for the triton. The total angular momentum of the two-body subsystem was restricted to  $j \leq 2$ . This led to 18 three-body channels in the channel-spin coupling.

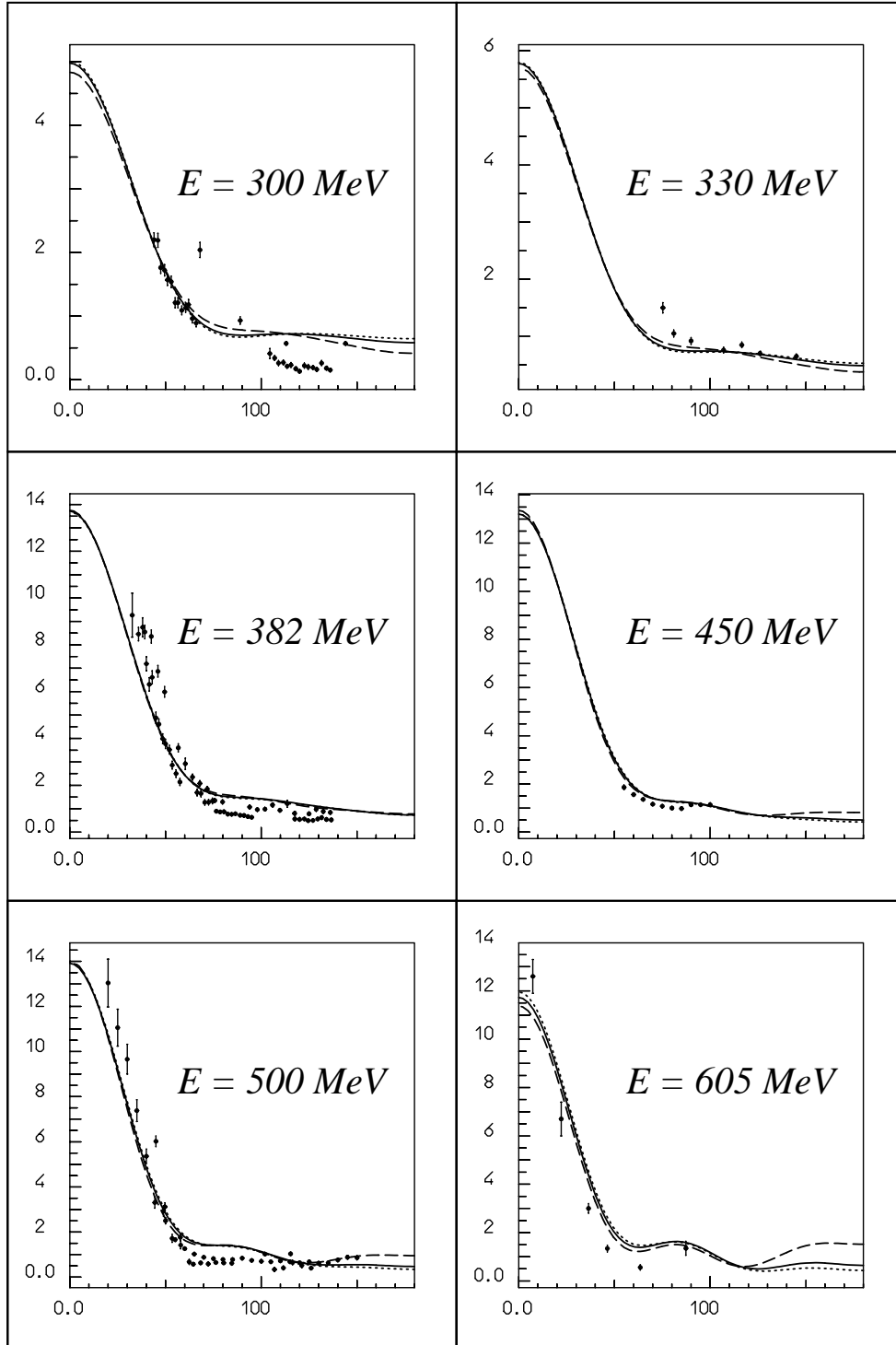




*Fig. 2 Canton PRC*



$\sigma(E, \theta) [pd \rightarrow \pi^+ t] \left( \frac{\mu b}{sr} \right)$



$\theta \text{ (deg)}$

Fig. 4 Canton PRC

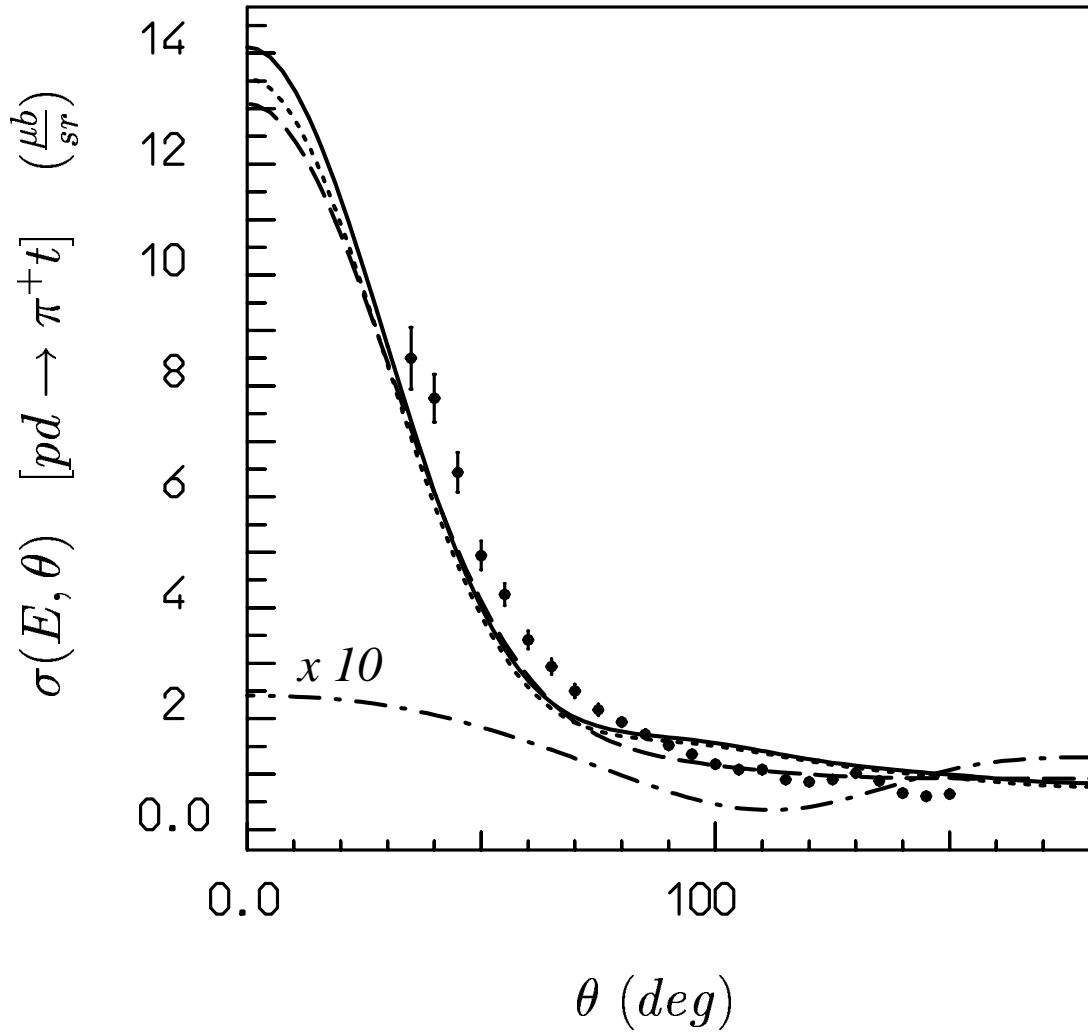


Fig. 5 Canton PRC

